A Large Parametric Finite Element Study of Pedestrian Injury Variability in the Current U.S. Vehicle Fleet

Jaehyuk Heo, Katarzyna Rawska, Neal Morgan, Bronislaw Gepner

Abstract This study presents a large parametric finite element simulation framework for systematically evaluating pedestrian injury variability across selected vehicle configurations. A total of 243 pedestrian impact simulations were conducted using validated FE vehicle models representing a sedan, SUV, and pickup truck. Simulations included three pedestrian anthropometries, as well as variations in vehicle impact speed and stiffness. Injury metrics relevant to lateral impacts were analysed using meta-modeling and variance-based sensitivity analysis to quantify the relative influence of parameters. Vehicle impact speed was the dominant factor influencing most injury metrics. Thoracic response depended strongly on vehicle type, with pickup trucks producing high chest loading even at 15 mph. Interaction effects between pedestrian anthropometry and vehicle front-end geometry were also identified: the AF05-SUV combination increased thorax loading, while AM50-SUV and AM95-SUV interactions showed elevated pelvis loading due to alignment of specific body regions with the hood leading edge. Thoracic response in pickup impacts showed limited sensitivity to hood and front-end stiffness, with average differences of 3.9% and 8.9% injury metric, respectively. These findings suggest that current pedestrian testing protocols may not capture thoracic injury risk from high hood leading edge vehicles.

Keywords Pedestrian safety, Vehicle front-end geometry, Human body model, Sensitivity analysis, Thorax injury

I. INTRODUCTION

The United States (U.S.) vehicle fleet is increasingly dominated by Sport Utility Vehicles (SUVs) and pickup trucks, accounting for 75% of new vehicle registrations in 2024 [1]. In 2025, 20 out of 25 best-selling cars were SUVs or pickup trucks (Fig. 1), and this trend is continuing in 2026 [2]. The list of best-selling vehicle models highlights the uniqueness of U.S auto market compared to Europe and most of the rest of the world.

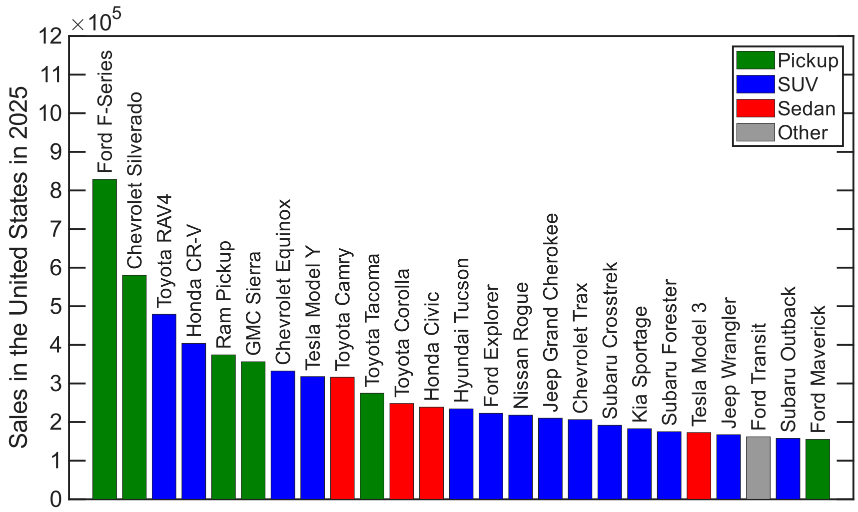

Fig. 1. The 25 best-selling cars in 2025 based on the data from Kelly Blue Book [2].

Jaehyuk Heo is a PhD student at the University of Virginia Center for Applied Biomechanics. Katarzyna Rawska is a Laboratory Specialist Senior at the University of Virginia Center for Applied Biomechanics, Neal Morgan is a Postdoctoral Research Associate at the University of Virginia Center for Applied Biomechanics, Bronislaw Gepner (bg5ah@virginia.edu, +1-434-297-8046) is a Research Associate Professor at the University of Virginia Department of Mechanical and Aerospace Engineering.

The U.S. fleet composition is particularly important for pedestrian safety because SUVs and pickup trucks typically have higher front-end profiles compared to sedan-type vehicles, causing different pedestrian kinematics and injury distributions. The idea of differences in pedestrian injury distribution between big/taller vehicles and passenger cars is supported by recent field data studies. In [3], the authors analysed 82 single-vehicle crashes from the Vulnerable road user Injury Prevention Alliance (VIPA) database and identified that SUVs are disproportionately dangerous to pedestrians when compared to sedans, specifically for the thigh and hip regions caused by impacts with features on the bumper, grille, or headlights. In [4], the authors analysed 202 pedestrian crashes to generate injury risk curve and revealed that Hood Leading Edge (HLE) height significantly increased the risk of pedestrian injury along with impact speed. In [5-6], the authors highlighted that relative HLE height compared to the pedestrians may be related to the pedestrian injury risk and severity for the head, torso, and hip. Although field data studies consistently show increased pedestrian injury risk associated with SUVs and pickup trucks, they are limited in defining the underlying injury mechanisms due to limited information using field data alone.

Recognising this, finite element (FE) studies have targeted the current U.S. vehicle fleet and conducted pedestrian reconstruction analyses to better understand variability in pedestrian injuries in real-world crashes [7-8]. In [7], the authors reconstructed five real-world pedestrian crashes from the Vulnerable Road User In-Depth Crash Investigation Study (VICIS) database and developed five morphed generic vehicle (GV) models representing U.S. vehicle front-end geometries. Based on responses from simplified pedestrian models developed by the Global Human Body Models Consortium (GHBMC), the results of the reconstruction matched well with the actual crash data. Similarly, in [8] the authors reconstructed three VICIS cases using fully deformable FE vehicle models, and the simulation outcomes showed good agreement with observed vehicle deformation patterns and injury outcomes using the Total Human Model for Safety (THUMS). The average prediction accuracy exceeded 85 % for AIS 2+ and AIS 3+ injuries across three vehicle types (one sedan, one SUV, and one pickup truck). While both studies provide valuable insights into specific real-world crash events, they are inherently specific case driven. As a result, their findings are difficult to generalise to a larger population and lack statistical representativeness. Moreover, this makes it hard to quantify sensitivity of injury to impact speed, pedestrian size, or variability in vehicle type. Given that pedestrian injury outcomes are influenced by interactions among multiple factors in real-world crashes, quantification can provide a basis for developing injury thresholds, design targets, physical test conditions for consumer rating protocols. Therefore, it is important to understand how injury outcomes change when input variables change and identify dominant or minor contributors to specific injury types that cannot be captured through a limited number of reconstruction cases.

The objective of this study is to systematically quantify the influence of vehicle and pedestrian characteristics on pedestrian injury outcomes associated with the current U.S. vehicle fleet. Using a parametric FE simulation framework and sensitivity analysis, the study evaluates the relative effects of vehicle type, impact conditions, and pedestrian anthropometry on pedestrian injury metrics. Moreover, this study investigates the interaction effects related to pedestrian height relative to vehicle geometry. In addition, the study tries to answer the question of applicability of the current pedestrian safety regulations, such as Euro NCAP to the contemporary U.S. vehicle population. This framework enables a structured comparison of multiple influencing factors, identifies dominant and secondary contributors to injury outcomes, reveals sensitivity rankings, and captures variability in pedestrian injury outcomes beyond what can be inferred from individual reconstruction cases.

II. METHODS

A large parametric simulation study was conducted using three specific FE vehicle models, which were evaluated against pedestrian impactor tests and real-world pedestrian crash reconstructions [8]. The vehicle models include three vehicle classes (one sedan, one SUV, and one pickup truck), and the Human Body Models (HBMs) cover three anthropometries: 5th percentile female (AF05), 50th percentile male (AM50), and 95th percentile male (AM95). The simulation matrix varied pedestrian anthropometry, impact speed, hood stiffness, and front-end stiffness resulting in a total of 243 simulations (TABLE I and TABLE II). To quantify pedestrian injuries, nine injury metrics spanning the head, thorax, pelvis, and lower extremities were calculated (TABLE III). Next, meta-modeling techniques and variance-based importance analysis, were applied to quantify the statistical significance and relative influence of each parameter on pedestrian injury outcomes.

Simulation Matrix

A full-factorial Design of Experiments (DOE) of pedestrian impact simulations was performed (TABLE I). Each parameter was defined at three levels for consistency across factors. A total of 243 simulations were performed using the THUMS v4.02 human body model.

TABLE I
SIMULATION MATRIX

Vehicle Type (FE model)	Hood Stiffness	Front-end Stiffness (Grille + Bumper)	Vehicle Speed [mph]	Anthropometry
Sedan (2015 Toyota Camry)	Soft	Soft	15	AF05
SUV (2020 Nissan Rogue)	Baseline	Baseline	25	AM50
Pickup truck (2014 Chevrolet Silverado)	Stiff	Stiff	35	AM95

Vehicle Type

Hereafter, “Sedan” refers to the 2015 Toyota Camry, “SUV” to the 2020 Nissan Rogue, “Pickup” to the 2014 Chevrolet Silverado used in this study. These vehicles were selected as representative examples of their classes. However, they do not statistically capture full variability within each vehicle category. To at least check whether these three vehicles are reasonably representative in terms of vehicle size, Principal Component Analysis (PCA) was performed using the dataset provided by IIHS, as described in Appendix G (Fig. G1 and Fig G2).

Vehicle Stiffness

Vehicle FE models were created for each category by modifying the stiffness of selected components in the baseline FE model, which are from the previous study [8]. Stiffness adjustments were made by changing the FE shell element thickness of the vehicle's outer and inner hood layers (blue), grille (red), and bumper (green) (TABLE II). The inner components in the grille and bumper region that may affect the pedestrian impact were also scaled using the same scaling factor.

TABLE II
DEVELOPED VEHICLE FE MODELS FOR THE THREE STIFFNESS CATEGORIES

Vehicle Stiffness Category	Pickup (2014 Chevrolet Silverado) 		SUV (2020 Nissan Rogue) 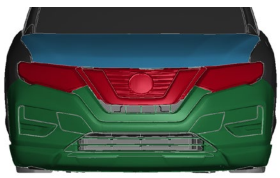		Sedan (2015 Toyota Camry) 	
	Hood	Grille + Bumper	Hood	Grille + Bumper	Hood	Grille + Bumper
	Scaling factor (for thickness)		*Scaling factor (for thickness)*		*Scaling factor (for thickness)*	
Soft	0.5	0.25	0.5	0.25	0.5*	0.25
Baseline	1	1	1	1	1	1
Stiff	2	4	2	4	2	4
# of FE vehicles	9		9		9	
Total # of vehicles models	27					

hood (parts marked in blue), grille (parts marked in red), bumper (parts marked in green)
*the hood thickness for the soft version of the Toyota Camry was borrowed from the Nissan Rogue.

Fig. E1-3 show the hood stiffness adjustment based on HIC_{15} score result. The target for the stiff configuration was to produce head impactor responses in which the majority of the Euro NCAP test locations resulted in HIC_{15} values exceeding 1700 based on the rating table (colored in red). Conversely, the soft configuration aimed to reduce HIC_{15} values below 650 (colored in green). For the Chevrolet Silverado and Nissan Rogue, the hood thickness was scaled up and down using a scaling factor of 2. However, for the Toyota Camry, a slightly different approach is required because the baseline model already has a very low hood thickness, which caused bottoming out in many impact locations. As a result, it was not possible to create the soft version of the model with consistent approach. To address this, the thickness value for the soft version of the Toyota Camry was copied from the Nissan Rogue (TABLE II). For the stiff hood of the Toyota Camry, a scaling factor of 2 was used without copying the value from the Nissan Rogue.

An analogous approach was applied to the grille and bumper assembly (Fig. E4-9). The stiffness of these components, including internal support structures influencing pedestrian leg impacts, was modified by scaling shell thickness relative to the baseline configuration (by a factor of 4). The resulting models were evaluated using Euro NCAP upper and lower legform impactor simulations. The objective was to establish three conditions corresponding to baseline performance, a stiffer configuration, and a softer configuration with a more compliant response, detectable using the reference impact tests. Because upper and lower legform responses are highly dependent on vehicle front-end geometry and shape, the goal was not to define strict pass/fail stiffness levels. Instead, the aim was to generate three distinct and clearly separable reference stiffness states that could be consistently distinguished using the impactor-based evaluation metrics.

Vehicle Speed

Three impact speeds that reflect common scenarios and injury outcomes, from minor to severe injuries, were considered. The 15 mph (24 km/h) speed shows that the likelihood of severe injury is low. Studies show pedestrians often survive with minor injuries or no injury [9-10]. This speed represents low-impact urban collisions. The 25 mph (40 km/h) speed is consistent with the Euro NCAP protocol for Vulnerable Road Users, which conducts tests at 25 mph [11]. Existing studies indicate that the risk of serious injuries increases at this speed [12]. This threshold is critical for pedestrian safety and aligns with international safety standards. Speeds above 30 mph significantly raise the risk of fatal injuries. At 35 mph, severe head and thoracic injuries become more likely [10][13]. Including this speed reflects high-severity collisions.

Pedestrian Pre-impact Posture and Orientation Relative to the Vehicle

All three pedestrian models were positioned in a mid-gait stance (50% of the gait cycle, with the left leg forward and the right leg back), aligned with the centreline of each vehicle and oriented laterally (Fig. 2 and Fig. 3). No pedestrian movement was assumed. This mid-gait stance was selected based on previous studies [14-15], which show that this posture best represents typical pedestrian movement during collisions. In [15], the author specifically explored how the position of the initially impacted leg influences upper body rotation and the point of initial head contact. For this study, left leg forward posture and right side impact were chosen.

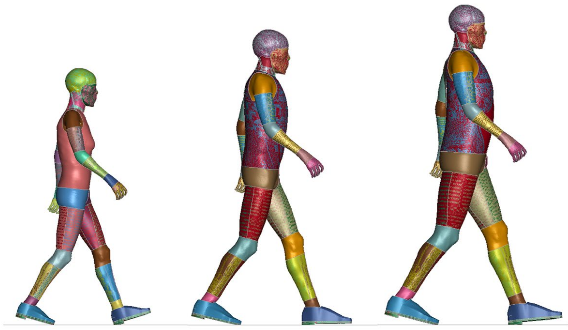

Fig. 2. Pedestrian anthropometries: AF05, AM50, and AM95 THUMS v4.02 models positioned in a mid-gait stance (from left to right).

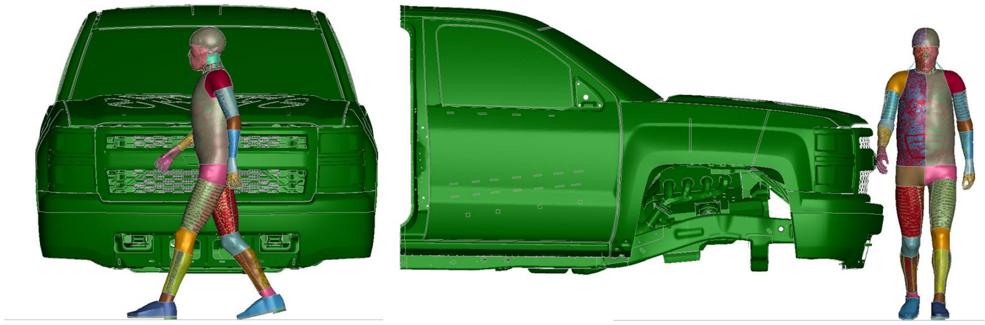

Fig. 3. Example of a vehicle-pedestrian impact simulation setup; the pedestrian (AM50) is laterally oriented and aligned with the vehicle (Pickup) centreline.

Injury Prediction

One of the advantages of using THUMS model is its ability to predict injury risk across multiple body regions by utilising the Human Injury Prediction Suite (HIPS), developed by the University of Virginia Center for Applied Biomechanics [16]. Although the tool covers more than 100 injury metrics for frontal and lateral impacts, this study focused on nine injury metrics because the cases involved pure lateral pedestrian impacts only. These output metrics can be used to directly calculate the injury risks using literature-based injury risk functions (TABLE III). However, the raw injury metric values were used when developing meta-modeling instead of the calculated injury risks, since many risk outputs were highly biased toward 0 or 1 for certain metrics (one example is shown in Fig. F1). This made it difficult to interpret how each parameter influenced injuries when analysing risk based on meta-modeling outcomes.

TABLE III
INJURY METRICS FOR INJURY RISK PREDICTION

Body Region	Detailed Body Region	Injury Metrics	Unit	Reference
Head	Skull	HIC_{15}	-	[17]
	Brain	BrIC	-	[18]
		DAMAGE	-	[19]
Thorax	Thorax	Cmax Lateral	-	[20]
Upper Extremity	Pelvis	Pubic Force	N	[21]
	Femur	Bending Moment	Nm	[22]
Lower Extremity	Knee	Lateral Bending Angle	Deg	[23]
	Tibia	Bending Moment	Nm	[22]
	Ankle	Lateral Bending Angle	Deg	[24]

Meta-Modeling

To evaluate the relative influence of the parametric study parameters on predicted pedestrian injury outcomes, a simplified meta-modeling approach was employed. The goal of meta-modeling is to create a model of a model to define the structure, rules, and relationships that a set of models must follow. By statistically mapping the relationship between input parameters and outputs (injury metrics in this study), the meta-model enables variable screening and quantifies the relative contributions of individual parameters to injury prediction. The primary objective of this process for our study is to identify which parameters are statistically significant in predicting pedestrian injury metrics and to prioritise those that should be targeted in real-world pedestrian safety efforts.

A linear regression model with first-order interaction terms was applied in this study (Equation 1). This model provides the minimum necessary complexity to identify parameters of primary influence and capture non-linear responses, while providing an interpretable structure. Using Matlab R2024b (MathWorks, Natick, MA) stepwise regression tool, the tool was employed to automatically select a set of predictor variables for a multiple regression model. It iteratively adds or removes variables based on statistical criteria like ANOVA p-value thresholds (5% for adding a term and 10% for removal in this study), for individual parameter coefficients, to select a model containing significant parameters. The intercept term was included to represent the minimum possible response within the parameter ranges of the test matrices. As part of the stepwise regression, forward inclusion as well as backwards elimination were employed to further enhance interpretability and reduce overfitting by removing less significant parameters. This method is commonly applied with screening designs to reduce the focus from many parameters of unknown relevance to a few parameters that drive the largest variation in response. Further studies can then direct efforts and resources more efficiently to the primary parameters of interest. Used linear regression model is defined as:

$$f(x_1, \dots, x_n) = \beta_0 + \sum_{i=1}^{n} \beta_i x_i + \sum_{i=1}^{n-1} \sum_{j=i+1}^{n} \beta_{ij} x_i x_j \quad (1)$$

where f is the analysed model, x_i is input variables, n is total number of input variables, β_0 is intercept, β_i is coefficient of first order (main effect) term and β_{ij} is coefficient of first order interaction term (interaction effect). Categorical parameters (vehicle type and anthropometry) were implemented using one-hot encoding. Continuous parameters (vehicle speed, hood stiffness, and front-end stiffness) were normalised and represented numerically using values of 0, 0.5, and 1 corresponding to low, baseline, and high levels (TABLE IV). The intercept represents the predicted response for the reference categorical levels (sedan and AM50) at the lowest levels of all continuous parameters.

TABLE IV
PARAMETER ENCODING SCHEME FOR META-MODEL DEVELOPMENT

Parameter	Levels	Encoding Method	Encoded Values
*Vehicle Type**	Sedan, SUV, Pickup	One-hot	(0,0), (1,0) (0,1)
*Anthropometry***	AF05, AM50, AM95	One-hot	(1,0), (0,0), (0,1)
Hood Stiffness	Soft, Baseline, Stiff	Numerical scaling	0, 0.5, 1
Front-end Stiffness	Soft, Baseline, Stiff	Numerical scaling	0, 0.5, 1
Vehicle Speed	15, 25, 35 mph	Numerical scaling	0, 0.5, 1

**Sedan used as reference category, **AM50 used as reference category*

Parameter Importance Analysis

Global sensitivity analysis was conducted to complement the interpretation of the fitted meta-models and to provide an additional assessment of parameter importance. In this study, a variance-based global sensitivity analysis framework proposed by [25] was adopted. This method has also been successfully applied to quantify the influence of design variables in aerodynamic design exploration, giving valuable insights for designers [26].

The adopted framework enables the computation of both Sobol' indices and Shapley values. The inclusion of Shapley values helps avoid the overcounting of interaction effects among input variables. Therefore, this approach provides a more robust basis for assessing parameter importance. In addition, the total contributions of all input parameters are normalised such that they add up to 1, which further enhances interpretability. In our study, Sobol' indices and Shapley values were calculated analytically, as the meta-model formulation was sufficiently simple to allow direct calculation. Interaction effects were quantified by subtracting the first-order Sobol' indices from the total effects estimated using Shapley values. Consequently, the approach enables the quantification of how much each individual variable contributes to the overall variability of the model output. In particular, the influence of first-order features on model performance can be evaluated.

III. RESULTS

A total of 243 simulations were performed in this study (Table I). The simulation time was set to 250 ms to ensure proper head contact with the hood or windshield. Among these, 4 out of 243 cases terminated early. However, the primary impact phase was completed in all cases after the head contacted the hood or windshield. Therefore, all cases were included in the following analysis.

Probability of Injury Risk (AIS 2+ and AIS 3+, AM50)

Before proceeding to the meta-modeling and sensitive analysis, the probability of pedestrian injury was evaluated only for the AM50 model, as anthropometric scaling factors for injury risk functions are still under development within the injury prediction suite. In addition, lower extremity injury risks were not included in the analysis shown in Fig. 4 and Fig. 5. Element deletion was activated for the knee ligaments to address numerical stability issues. Ligament rupture following knee contact with the vehicle front-end resulted in large knee rotations accompanied by relatively small femur and tibia moments, which caused the injury risks to converge toward extreme values (i.e., near 0 or 1) in many simulations. Based on these considerations, injury risk evaluation was limited to the head, thorax, and pelvis, although lower extremity responses still provided useful information for sensitivity analysis. Figures 4 and 5 Show the predicted AIS 2+ and AIS 3+ injury probabilities for the head (skull and brain), thorax, and pelvis across three vehicle types (sedan, SUV, and pickup) at impact speeds of 15, 25, and 35 mph. Injury risks were calculated using HIC_{15} and DAMAGE metric for the head, lateral chest deflection (Cmax lateral) for the thorax, and pubic force for the pelvis.

Overall, the predicted pedestrian injury risks increase with impact speed across all body regions, although the sensitivity to vehicle type varies (Fig. 4, Fig. 5). For the head (skull), injury risk remains low at 15 mph (below 15%) but increases sharply at 25 mph and reaches nearly 100 % at 35 mph for all vehicle types. Sedans show higher risk than SUVs and pickups at 15 mph and 25 mph. In contrast, brain injury risk shows already moderate risk at 15 mph for sedans and SUVs but remains low for pickups. However, at 25 mph and above, brain injury risk becomes saturated (≈100 %) for all vehicle types. The thorax shows strong dependence on vehicle type. Pickups with AM50 produce extremely high injury probabilities even at 15 mph. Sedans and SUVs exhibit more gradual increases as speed increases. Regardless of vehicle speed, the thorax injury risks reach nearly 100 % in pickup-pedestrian impacts. For the pelvis, injury risk remains generally low for sedans and pickups but increases substantially for SUVs, particularly at 25 mph and 35 mph.

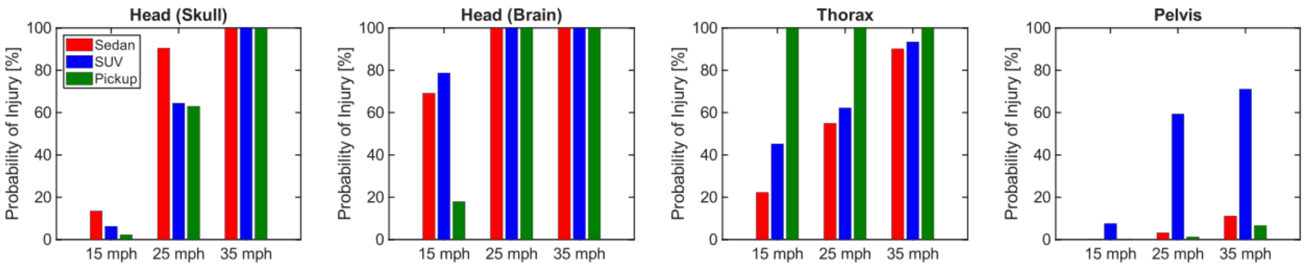

Fig. 4. Predicted probability of AIS 2+ pedestrian injury for head, thorax, and pelvis across vehicle types and impact speeds for AM50 pedestrian model.

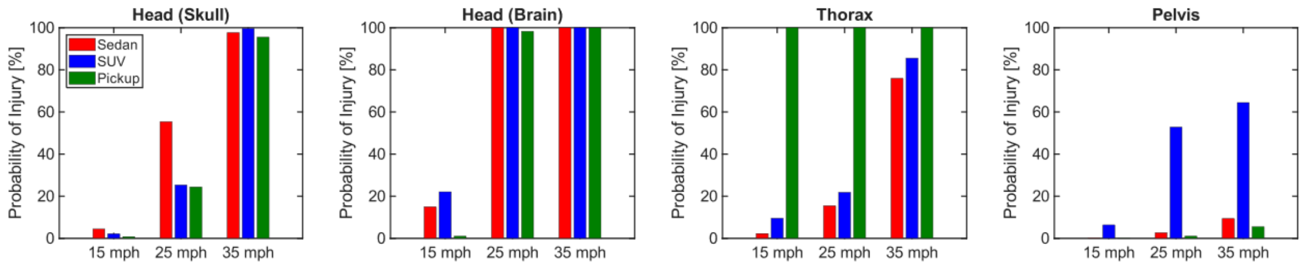

Fig. 5. Predicted probability of AIS 3+ pedestrian injury for head, thorax, and pelvis across vehicle types and impact speeds for AM50 pedestrian model.

Meta-Modeling

Separate meta-models were developed for each selected injury metric. Figures A1 and B1 show the predictive performance of the meta-models for nine injury metrics and corresponding estimated regression coefficients respectively. Each scatter plot compares the meta-model prediction (y-axis, predicted value) against the corresponding simulation result (x-axis, true value), where the 45° diagonal line represents perfect prediction.

The predictive capability of meta-models was quantitively evaluated using adjusted R^2 and RMSE and visually assessed by checking how closely the data points fall around the perfect prediction line. A total of 243 datapoints are included in the figures, color-coded by vehicle type (Sedan, SUV, Pickup) and distinguished by marker type to indicate pedestrian anthropometries (AF05, AM50, AM95).

Overall, the meta-models show good predictive capability. Injury metrics such as BrIC, Cmax lateral, pubic force and tibia moment exhibit high adjusted R^2 values near 0.9 or above. Other responses show greater variability but maintain adjusted R^2 values close to 0.8. For certain metrics, including pubic force and ankle angle, clustering of data points is observed, likely due to the limited number of input variables and the low resolution of their parameter ranges in the simulation matrix. For example, variations in hood stiffness have minimal influence on ankle angle, resulting in nearly identical responses across cases with stiff, baseline, and soft hood when combined with stiff front-end. Nonlinear behavior or outliers are also evident for certain metrics. Nevertheless, the meta-models shown in Fig. A1 successfully capture the overall response trends across all injury metrics.

Parameter Importance

Figure 6 shows the relative contribution of each input parameter to the predicted injury metrics across different body regions. The sedan vehicle type and AM50 anthropometry are not shown in the figure because they were used as reference categories. The effects of the SUV and pickup vehicle type were evaluated relative to the sedan, while AF05 and AM95 anthropometries were evaluated relative to the AM50. The yellow bars represent the main (first-order) effects, while the dark gray portions indicate interaction effects associated with each first-order parameter. Overall, impact speed is consistently identified as the most influential parameter for injury metrics. An exception is observed for Cmax lateral, for which pickup vehicle type is the dominant factor. Anthropometric factors and vehicle stiffness generally exhibit smaller but still non-negligible contributions. It suggests that their influence is primarily shown through interaction effects rather than through main effects.

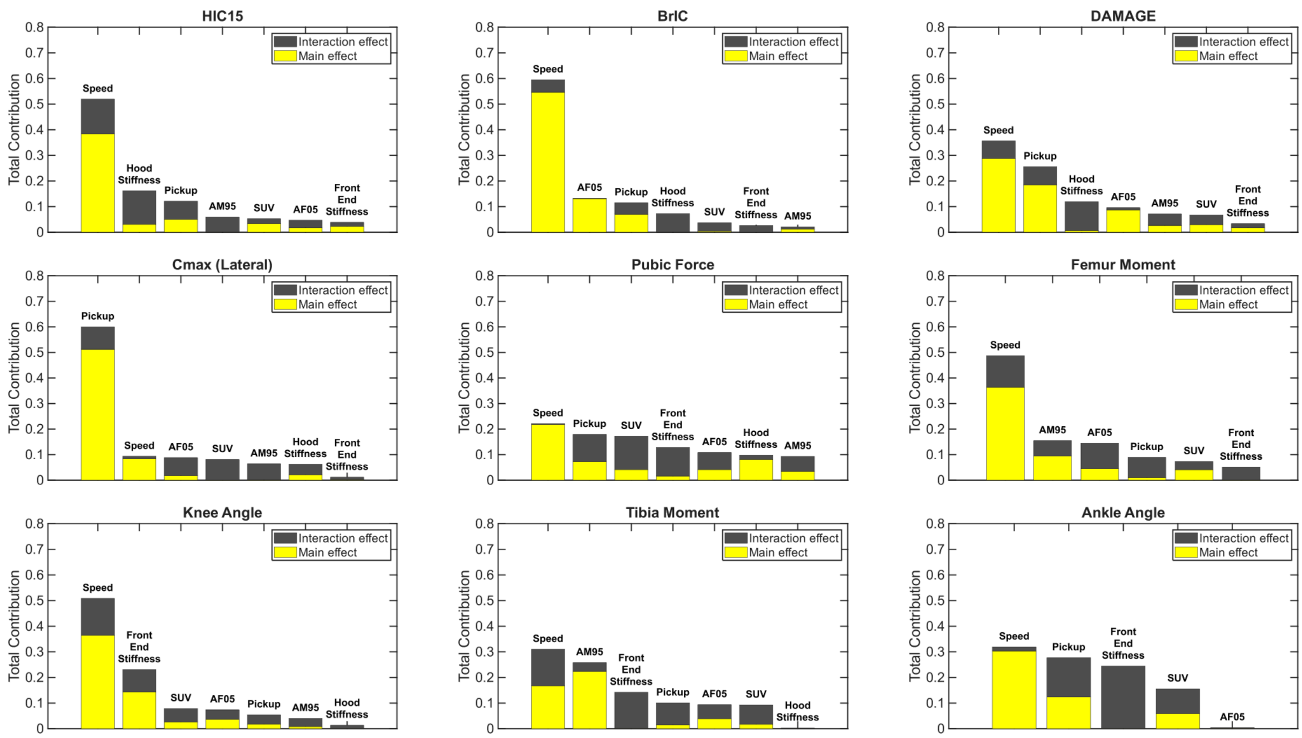

Fig. 6. Relative contributions of input parameters to the predicted injury-related responses. The sum of all parameter contributions is equal to 1. Yellow bars represent the main effects of the input parameters, whereas gray bars represent their interaction effects. The total contribution of each parameter was quantified using the Shapley value, which includes both the main effects (Sobol' indices) and interaction effects. Thus, the interaction effect was computed as the difference between the Shapley value and the main effect [25][26].

Interaction Effect (Pedestrian Height Relative to the Vehicle)

Figures C1, C2, and C3 show tile plots showing median values of selected injury metrics. Each tile includes 27 cases and highlights the interaction effects between two input parameters. Among these plots, Cmax lateral and pubic force exhibit notable and clear interaction patterns across anthropometry and vehicle type (Fig. 7). For the thorax, the AF05 is the only anthropometric group that shows values more than two times higher for the SUV compared to the sedan, whereas AM50 and AM95 remain relatively similar between the two vehicle categories. In addition, the pickup generally increases the overall Cmax lateral across all pedestrian sizes, however the increase for the AM95 is lower than for the other two anthropometries. For the pelvis, AM50-SUV and AM95-SUV cases show higher pubic forces than sedan and pickup cases, whereas AF05-SUV cases show lower pubic force.

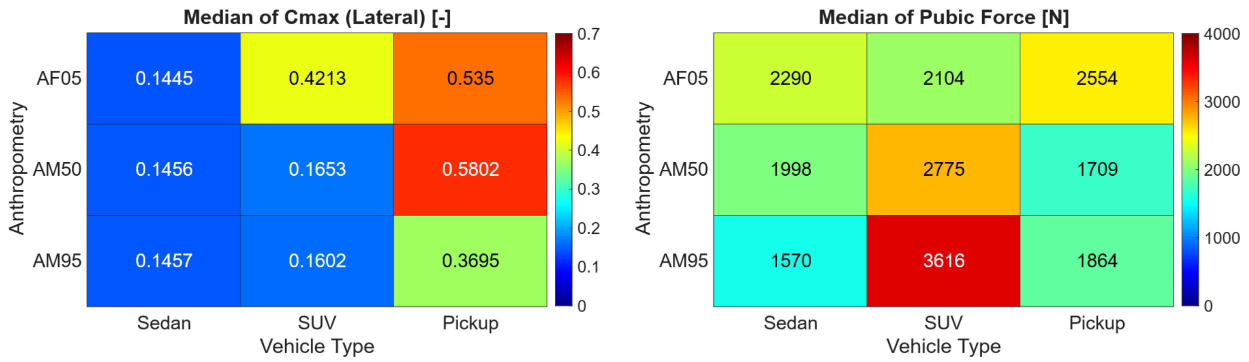

Fig. 7. Median of Cmax lateral (left) and pubic force (right) across anthropometry and vehicle type. Each tile represents the median value from 27 simulations in this study. For example, AF05-SUV tile shows the median value calculated from the 27 simulations including all impact velocities and stiffness settings.

IV. DISCUSSION

The issue of pedestrian injuries associated with vehicles with high hood leading edges and heavy SUVs or trucks has been signaled before [27-32]. As pedestrian fatalities are on the rise in the U.S., unlike other developed nations such as the European Union (EU) and Japan, there is a need to better understand pedestrian safety within the current U.S. vehicle fleet. It is necessary to determine whether current pedestrian safety protocol is feasible and, if not, which parameters should be prioritised and what alternative approaches may be effective means of improving pedestrian safety.

Injury Prediction

Predicted AIS 2+ and 3+ injury risks for the AM50 pedestrian increased substantially at 25 mph compared to 15 mph for the head (skull), brain, and pelvis [Fig. 4, Fig. 5]. With the exception of pickup impacts, which produced extremely high thorax injury risks even at 15 mph (low speed), predicted thorax injury risk also showed a gradual increase, exceeding a 50% AIS 2+ injury risk at 25 mph. Interestingly, epidemiological data in the U.S. indicates that 68.7 % of pedestrian injury cases occurred at speeds of 25 mph (40 kph) and below [33]. This consistent trend builds confidence in injury prediction using HBM and the proposed test speed of 25 mph in NCAP.

Additionally, a meta-model with the minimum necessary complexity was able to reasonably predict pedestrian injury outcomes [Fig. A1]. It indicates that the model explains well their relationship between varied parameters and outcomes. This verifies that the dataset may be adequate for meta-modeling and sensitivity study. However, it is important to note that only three vehicles were considered. Therefore, adding more vehicle models would improve the ability to capture injury variability representative of the current U.S. vehicle fleet, especially, given that 20 out of 25 best-selling vehicles are SUVs or pickup trucks manufactured by different auto makers.

Analysing the meta-models, response revealed several key observations. First, for HIC, hood stiffness emerged as the second most influential parameter after vehicle speed (Fig. 6). This is a positive finding, as hood stiffness is currently evaluated through impactor tests in existing pedestrian protection regulations. It should be noted that the head of the HBMs contacted the windshield or cowl in many cases, particularly for sedan configurations and at 35 mph (Fig. D1). Since the stiffness of the windshield and cowl was not varied, the stiffness of the structures contacting the head may be underestimated, although the results remain informative. Additionally, a protective effect was observed for SUV and pickup truck, particularly in combination with AF05 anthropometry (Fig. B1, Fig. C1). Taller vehicles, when interacting with smaller pedestrians, tend to promote a transition from wrap-around kinematics to forward projection. This observation is consistent with findings from field data studies [5]. This shift may reduce head impact severity or, in some cases, prevent head contact altogether.

BrIC and DAMAGE, both used to predict brain injury, exhibit similar trends. In both models, vehicle speed is the dominant parameter, followed by AF05 anthropometry, vehicle type (pickup), and hood stiffness, which are consistently identified as the next most influential factors (Fig. 6). This alignment indicates strong agreement between the two prediction approaches. The protective effects associated with AF05 and pickup configurations are also consistent with the trends observed for HIC (Fig. B1). Specifically, the transition to forward projection kinematics reduces head angular motion, lowering predicted brain injury risk.

As pedestrian size increases, the bending moment in the femur and tibia regions tends to increase as shown in the scatter plots (Fig. A1) and tile plots (Fig. C1). It is likely associated with differences in lower extremity inertia between the models. For example, AM95 pedestrian generally has longer bones with thicker flesh, which results in a larger moment arm and larger bending moment. However, this does not necessarily indicate that AM95 pedestrians experience higher injury risk. Considering that AM95 has larger cross-sectional area and greater cortical thickness, an anthropometric scaling factor (e.g. through IRF) should be incorporated into the injury prediction suite.

Interaction Effect

In the pelvis region, SUV-AM50 and SUV-AM95 interactions are associated with increased pubic force (Fig. 7) and the SUV-AM50 combination exceeds a 50% probability of AIS 3+ pelvis injury (Fig. 5). The tile plot (Fig. 7) shows that SUV cases behave very differently. AM50 and AM95 struck by the SUV exhibits higher median value of pubic force compared to sedan and pickup. Figure 10 helps explain this result. Similar to the observation in Fig. 8, the SUV's hood leading edge aligns directly with the pelvis region for AM95 and closely for AM50, resulting in a more concentrated and direct impact load. This interaction between the hood leading edge and the pelvis explains the substantially higher pubic force observed for AM95 in the SUV case. In contrast, for AF05, the hood leading edge contacts higher regions above pelvis, therefore reducing the effective loading on the pelvis.

In the thorax region, SUV-AF05 interaction was associated with elevated Cmax lateral response (Fig. 7). Figure 8 helps explain the reason why AF05 shows a higher median value of Cmax lateral, particularly in the SUV case. For AF05 impacted by the SUV, the hood leading edge is positioned at approximately the same height as the torso region. This combination results in more direct loading to the chest, leading to greater torso injury. In contrast, AM95 impacted by pickup exhibit relatively lower than other pickup cases, even lower than SUV and AF05 combination. Figure 9 explains the reason that the hood leading edge of pickup impacts below the rib cage.

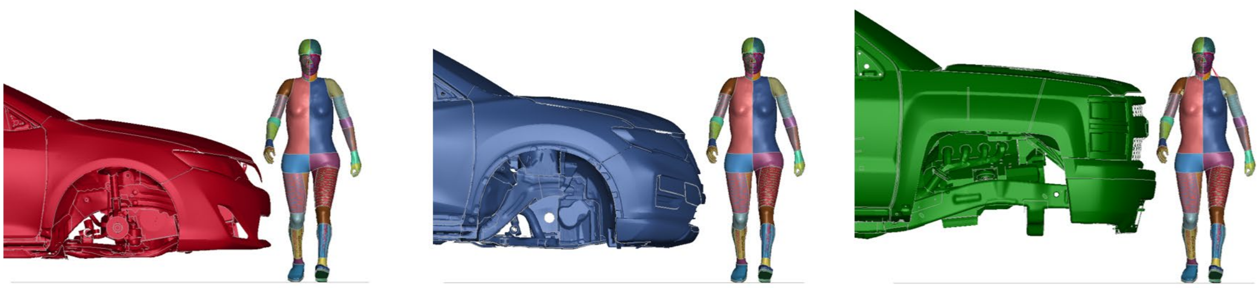

Sedan AF05 | SUV AF05 | Pickup AF05

Fig. 8. Simulation setup for AF05 impacts with different vehicle types.

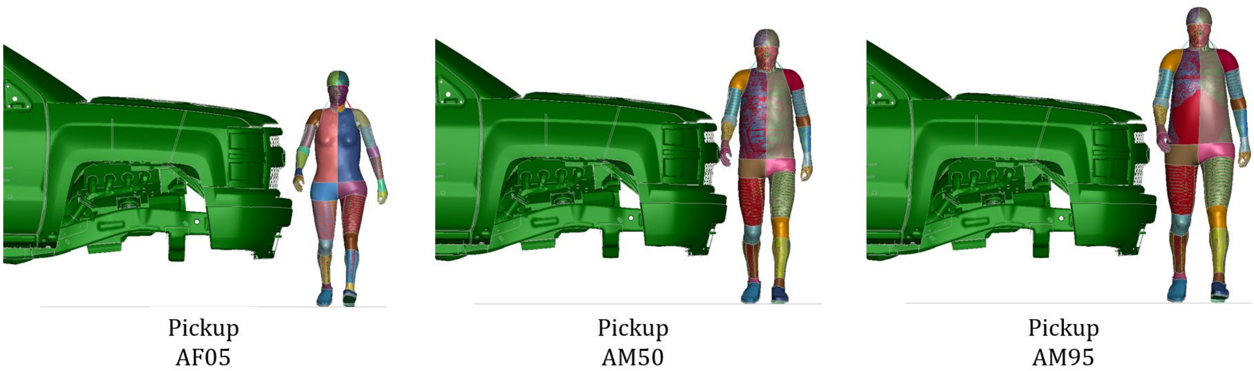

Fig. 9. Simulation setup for pickup impacts with different anthropometries.

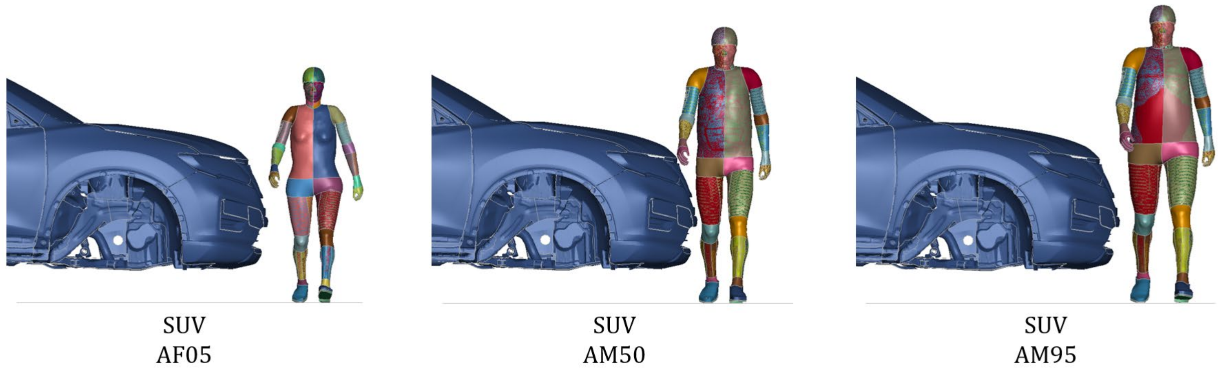

Fig. 10. Simulation setup for SUV impacts with different anthropometries.

These observations are important because they show that certain pedestrian populations may be more vulnerable in specific vehicle classes. It suggests that a single representative pedestrian may underestimate pedestrian injuries across different pedestrian sizes. It supports the need for more diverse pedestrian anthropometries in injury assessment, similar to the efforts in occupant safety.

Dominant Parameters on Pedestrian Injuries

Vehicle impact speed is most influential parameter across all injury metrics, except for the Cmax lateral, which is indicator of thorax injury (Fig. 6). This is closely aligned with the previous study [4]. The authors analysed 202 pedestrian crashes from U.S. roads, and updated estimate of pedestrian injury risk at different severity levels. They found that impact speed strongly increased the risk of pedestrian injury followed by hood leading edge height. In other words, delta-V reduction may be the most effective way to reduce pedestrian injuries and fatalities assuming that there is lack of countermeasure. However, for the thorax, our study shows that the specific factor of pickup truck is dominant contributor, explaining about 60 % of the total variation on Cmax lateral in the model. Even at 15 mph, pickup produces substantial Cmax value (Fig. 4, Fig. 5, and Fig. C4). This finding is aligned well with previous study [34]. The authors explored the effectiveness of active safety system (Pedestrian Automatic Emergency Braking; PedAEB) in reducing injury risk. Delta-V reduction from PedAEB was estimated to be very effective for head, pelvis, femur, and lower extremities. However, it was less effective in reducing the risk of thorax injuries. These studies support the need for continuing passive safety research into pedestrian thorax injury when pedestrians are struck by SUVs and pickup trucks.

Passive Safety: Impactors

NCAPs are expected to continue using subsystem impactors (headform, upper legform and lower legform) in their testing protocols, as they provide repeatable results at relatively low cost. Recent studies have also discussed the development of advanced lower leg impactors such as TRL (2003), FlexPLI (2014), and aPLI (2023). However, there remains a lack of impactors for pelvis and thorax regions, which may represent primary sources of injury for pedestrians in the contemporary U.S. vehicle fleet.

Recognising the limitations in assessing thorax injury risk using current impactors, thorax impactor prototypes proposed by [35–36] have been suggested as tools to predict thorax injuries. However, consensus on their adoption has not yet been reached, because it is still prototyping phase and should be validated using the reference value with cadaver or HBM simulation data. In [37], the authors suggested that headform impactor responses could serve as an alternative predictor of thorax injury risk, while [38] extended this hypothesis by considering various parameters such as pedestrian orientation, posture, lateral offset, and active bonnet systems. Since the headform impactor is designed to capture local hood stiffness characteristics, it may provide an alternative means of evaluating thorax injury risk in sedan or European-style vehicle fleets, where thorax contact with the vehicle hood after initial impacts to the lower extremities and pelvis. It may also be effective means of evaluating pelvis injury, given that pubic force is highly sensitive to hood stiffness and front-end stiffness (Fig. 11).

However, Fig. 11 shows that Cmax lateral in all vehicle types was not sensitive to hood stiffness and front-end stiffness. Instead of vehicle stiffness, vehicle type itself had a greater influence on Cmax due to direct thorax loading against the hood leading edge. Consistent with this, hood stiffness and front-end stiffness were ranked as the least influential parameters when predicting Cmax lateral (Fig. 6). These findings suggest that current pedestrian testing protocol may not be applicable for evaluation of thoracic injuries. It raises questions about whether thorax-specific impactor or alternative assessment approach is necessary.

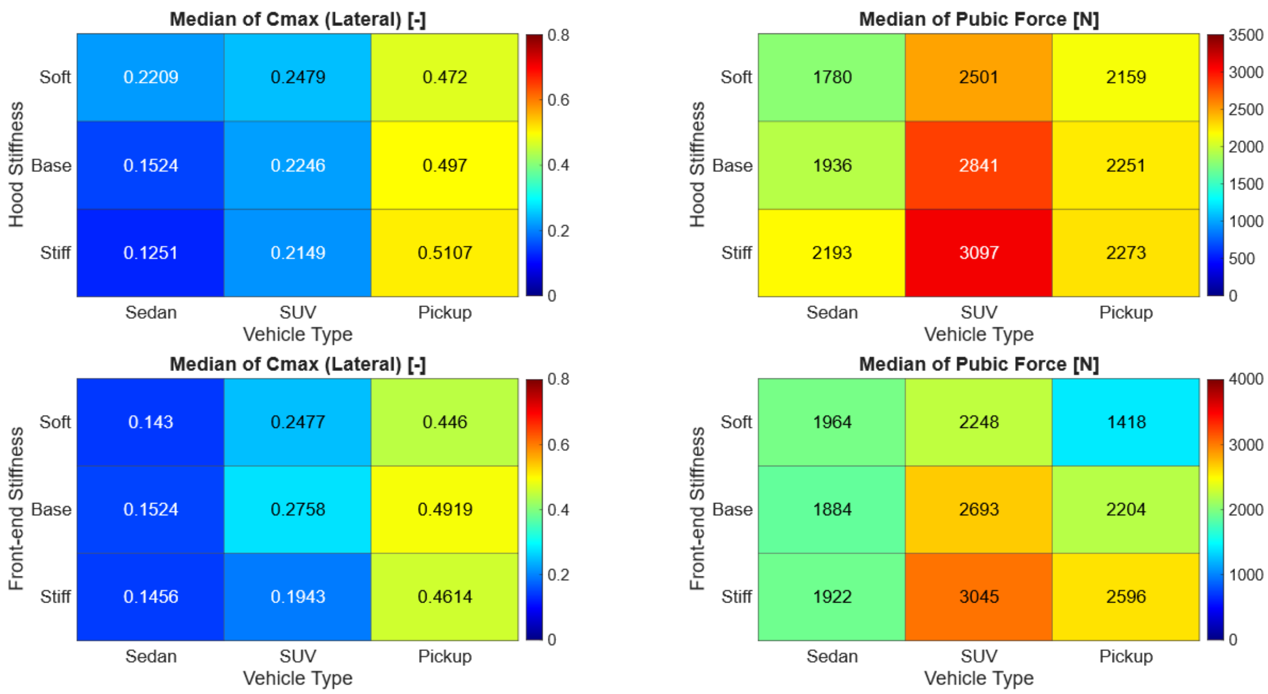

Fig. 11. Median of Cmax lateral and pubic force across hood stiffness, front-end stiffness, and vehicle type. The value shown in each tile represents the median value of 27 simulations, including all pedestrian anthropometries.

Limitations and Future Directions

First, this study considered only three specific vehicle classes. This is sufficient for a parametric comparison of selected representative cases, but it is not strong enough to support broader fleet-level conclusions. Three vehicles were selected representative examples of the current U.S. vehicle fleet and effectively cover the range of vehicle height-related characteristics (Fig. G1 and Fig. G2). However, three vehicles do not cover the range of front-end shape (or front-end slope), that can be categorized by blunt and sloped [40]. The present evidence does not fully separate class-level effects from model-specific geometric or structural effects. Rather, this study shows the effect of vehicle height on pedestrian injuries. In addition, the parameter rankings cannot be transferred directly to real-world importance. These findings quantify relative influence within the selected vehicle models, parameter ranges, and modeling assumptions.

Secondly, windshield stiffness was not varied. It may be particularly important for sedans or small SUVs, given that HBM's head predominantly contacted the pickup hood in the simulations (Fig. D1). However, the objective of this study was not to directly compare head injuries among vehicle types, but rather to quantify the relative importance of vehicle and pedestrian parameters on injury outcomes across a broad range of scenarios. If the head contacts the windshield that was not varied, the resulting response is primarily influenced by factors that determine the contact location, such as pedestrian anthropometry and vehicle type. Future studies incorporating windshield and cowl stiffness would help to quantify the contribution of these parameters to injury outcomes.

Finally, the parametric study used a limited number of input variables and coarse parameter ranges. They are intentionally chosen to simplify the process and capture the overall response trends. At this stage of this study, the objective was to understand the global sensitivity and interaction behavior of the variables. Future studies may consider finer variables, such as the more detailed ranges of hood leading edge height or hood angle to further investigate the effect of vehicle geometry and optimize the vehicle design for pedestrian safety.

V. CONCLUSION

This study examined the pedestrian injury variability across a set of selected vehicle configurations. Using a large parametric simulation framework and sensitivity analysis, the study quantified the relative influence of selected parameters on predicted injury outcomes. The key conclusions from this study are as follows:

- While the vehicles evaluated are representative of their respective classes, as confirmed by the PCA results, each is characterized by specific geometric features that may influence the predicted injury metrics. Nevertheless, several key findings are directly attributable to geometric characteristics that are fundamental to the vehicle class itself, such as hood leading-edge geometry. Consequently, these results may be interpreted as representative of broader trends associated with the corresponding vehicle classes rather than solely the individual vehicles examined.
- Vehicle impact speed was the most influential parameter for most injury metrics within the investigated parameter range. An exception was Cmax lateral, for which vehicle front-end geometry, particularly the hood leading edge height, showed the largest contribution to response variability.
- Thorax response appeared to be more strongly associated with vehicle type. In pickup impacts, severe thorax loading was predicted even at an impact speed of 15 mph, however, thorax response showed less sensitivity to hood and front-end stiffness variations. This suggests that the thorax response is associated with front-end profile, rather than stiffness variations.
- The proposed framework captured interaction effects of pedestrian height relative to vehicle geometry (pedestrian interaction with hood leading edge) that have previously been identified in field data studies. This analysis quantified trends with broader range of parameters and found:
    - SUV-AF05 interaction was associated with increased thoracic injury.
    - SUV-AM50 and SUV-AM95 interactions were associated with increased pelvis injury.
    - Pickup-AM95 interaction showed relatively lower thorax response compared with the other pickup-pedestrian combinations.

Beyond the specific injury trends observed in this study, this study developed a unified parametric simulation framework that enables a structured and consistent comparison of multiple factors influencing pedestrian injury outcomes. By evaluating vehicle type, impact speed, pedestrian anthropometry, hood stiffness, and front-end stiffness within a consistent design space and at comparable parameter levels, the framework allows the relative importance of individual factors and their interactions to be quantified systematically. This approach provides a basis for identifying dominant and secondary contributors to pedestrian injury variability and may support future efforts to prioritize design parameters and evaluation strategies for pedestrian protection.

VI. ACKNOWLEDGEMENTS

The author gratefully acknowledges the NHTSA for sponsoring this research and providing insightful feedback that supported the development and validation of the simulations presented in this study. The author also gratefully acknowledges the IIHS for providing a large vehicle measurement dataset that helped establish the representativeness of the U.S. vehicle fleet considered in this study.

REFERENCES

[1] THE SHOP. (2024) Report: SUVs & Trucks Set New Sales Record in 2024, THE SHOP. Available online.

[2] Kelley Blue Book. (2026) The 25 best-selling cars, trucks, and SUVs, Kelley Blue Book. Available online.

[3] Monfort, S. S., Mueller, B. C. (2020) Pedestrian injuries from cars and SUVs: Updated crash outcomes from the Vulnerable Road User Injury Prevention Alliance (VIPA). *Traffic Injury Prevention*, **21**(sup1): pp.S165–S167.

[4] Monfort, S. S., Mueller, B. C. (2025) A modern injury risk curve for pedestrian injury in the United States: The combined effects of impact speed and vehicle front-end height. *Journal of Safety Research*, **94**: pp.235–241.

[5] Mueller, B. C., Monfort, S. S., Jermakian, J. S. (2024) Role of pedestrian waist and hip height relative to the vehicle front end in kinematics and torso injuries, Stapp Car Crash Conference Short Communication.

[6] Monfort, S. S., Hu, W., Mueller, B. C. (2024) Vehicle front-end geometry and in-depth pedestrian injury outcomes. *Traffic Injury Prevention*, **25**(4): pp.631–639.

[7] Poveda, L., Miller, L. E., *et al.* (2025) Real-world pedestrian crash reconstructions: Vehicle model validation and biomechanical injury analysis. *Traffic Injury Prevention*, **26**(sup1): pp.S190–S201.

[8] Heo, J., Kong, J. S., *et al.* (2025) Pedestrian impact analysis considering U.S. vehicle fleet: Crash reconstruction and validation study using VICIS database. Proceedings of the IRCOBI Conference, 2025, Vilnius, Lithuania.

[9] Rosén, E., Stigson, H., Sander, U. (2011) Literature review of pedestrian fatality risk as a function of car impact speed. *Accident Analysis & Prevention*, **43**(1): pp.25–33.

[10] Tefft, B. C. (2013) Impact speed and a pedestrian's risk of severe injury or death. *Accident Analysis & Prevention*, **50**: pp.871–878.

[11] EuroNCAP. (2020) Vulnerable Road Users Protocol, EuroNCAP.

[12] Insurance Institute for Highway Safety. "Vehicle height compounds dangers of speed for pedestrians", www.iihs.org/news/detail/vehicle-height-compounds-dangers-of-speed-for-pedestrians [06 Apr 2026].

[13] Insurance Institute for Highway Safety. "Fatality Facts 2020 Pedestrians", www.iihs.org/topics/fatality-statistics/detail/pedestrians#yearly-snapshot [02 Dec 2022].

[14] Untaroiu, C. D., Meissner, M. U., *et al.* (2009) Crash reconstruction of pedestrian accidents using optimization techniques. *International Journal of Impact Engineering*, **36**(2): pp.210–219.

[15] Pak, W., Grindle, D., Untaroiu, C. (2021) The influence of gait stance and vehicle type on pedestrian kinematics and injury risk. *Journal of Biomechanical Engineering*, **143**(10): p.101007.

[16] Morgan, N., Lovenduski, C., *et al.* (2026) Instrumentation and analysis of THUMS simulations for whole body injury prediction. Proceedings of the Enhanced Safety of Vehicles Conference, 2026, Toronto, Ontario, Canada.

[17] Eppinger, R., Kuppa, S., *et al.* (2000) Development of improved injury criteria for the assessment of advanced automotive restraint systems: II, National Highway Traffic Safety Administration, Washington, DC.

[18] Takhounts, E. G., Craig, M. J., *et al.* (2013) Development of brain injury criteria (BrIC). Proceedings of the Stapp Car Crash Conference, 2013, Orlando, Florida, USA.

[19] Gabler, L. F., Crandall, J. R., Panzer, M. B. (2019) Development of a second-order system for rapid estimation of maximum brain strain. *Annals of Biomedical Engineering*, **47**(9): pp.1971–1981.

[20] Kuppa, S. (2004) Injury criteria for side impact dummies, National Highway Traffic Safety Administration, Washington, DC.

[21] Petitjean, A., Trosseille, X., *et al.* (2009) Injury risk curves for the WorldSID 50th male dummy. Proceedings of the Stapp Car Crash Conference, 2009, Savannah, Georgia, USA.

[22] Kerrigan, J. R., Drinkwater, D. C., *et al.* (2004) Tolerance of the human leg and thigh in dynamic latero-medial bending. *International Journal of Crashworthiness*, **9**(6): pp.607–623.

[23] Ivarsson, J., Lesley, D., *et al.* (2004) Dynamic response corridors and injury thresholds of the pedestrian lower extremities. Proceedings of the IRCOBI Conference, 2004, Graz, Austria.

[24] Funk, J. R., Srinivasan, S. C., *et al.* (2002) The effects of axial preload and dorsiflexion on the tolerance of the ankle/subtalar joint to dynamic inversion and eversion. Proceedings of the Stapp Car Crash Conference, 2002, Ponte Vedra Beach, Florida, USA.

[25] Owen, A. B. (2014) Sobol' indices and Shapley value. *SIAM/ASA Journal on Uncertainty Quantification*, **2**(1): pp.245–251.

[26] Palar, P. S., Zuhal, L. R., Shimoyama, K. (2023) Global sensitivity analysis in aerodynamic design using Shapley effects and polynomial chaos regression. *IEEE Access*, **11**: pp.114825–114839.

[27] Atkins, R. M., Turner, W. H., *et al.* (1988) Injuries to pedestrians in road traffic accidents. *British Medical Journal*, **297**(6661): pp.1431–1434.

[28] Ballesteros, M. F., Dischinger, P. C., Langenberg, P. (2004) Pedestrian injuries and vehicle type in Maryland, 1995–1999. *Accident Analysis & Prevention*, **36**(1): pp.73–81.

[29] Lefler, D. E., Gabler, H. C. (2004) The fatality and injury risk of light truck impacts with pedestrians in the United States. *Accident Analysis & Prevention*, **36**(2): pp.295–304.

[30] Ivarsson, B. J., Henary, B., *et al.* (2005) Significance of adult pedestrian torso injury. *Proceedings of the Association for the Advancement of Automotive Medicine*, **49**: pp.263–277.

[31] Desapriya, E., Subzwari, S., *et al.* (2010) Do light truck vehicles impose greater risk of pedestrian injury than passenger cars? A meta-analysis and systematic review. *Traffic Injury Prevention*, **11**(1): pp.48–56.

[32] Edwards, M., Leonard, D. (2022) Effects of large vehicles on pedestrian and pedalcyclist injury severity. *Journal of Safety Research*, **82**: pp.275–282.

[33] National Highway Traffic Safety Administration. (2024) New Car Assessment Program Final Decision Notice – Crashworthiness Pedestrian Protection, U.S. Department of Transportation, Washington, DC.

[34] Hu, J., Flannagan, C., *et al.* (2023) Understanding the new trends in pedestrian injury distribution and mechanism through data linkage and modeling. *Accident Analysis & Prevention*, **188**: p.107095.

[35] Zander, O., Wisch, M., *et al.* (2019) Development and evaluation of a thorax injury prediction tool (TIPT) and possibilities for incorporation within improved test and assessment procedures – results from SENIORS. Proceedings of the Enhanced Safety of Vehicles Conference, 2019, Eindhoven, The Netherlands.

[36] Chang, Y., Long, Y., *et al.* (2024) A study on the performance of WorldSID thorax module for thorax injury prediction in e-Bike rider based on real accident data. *Acta of Bioengineering and Biomechanics*, **26**(3): pp.171–181.

[37] Han, Y., Yang, J., Mizuno, K., Matsui, Y. (2012) A study on chest injury mechanism and the effectiveness of a headform impact test for pedestrian chest protection from vehicle collisions. *Safety Science*, **50**(5): pp.1304–1312.

[38] Jani, D., Staack, H., & Teichmann, C. (2025). Integrated Head and Thorax Protection Evaluation for VRU Safety: A Simulation Based Approach. In *IRCOBI Conference*.

[39] Park, G., & Kent, R. (2020). Foot shape analysis of professional American Football players. Footwear Science, 12(3), 153-159.

[40] Hu, W., Monfort, S. S., & Cicchino, J. B. (2024). The association between passenger-vehicle front-end profiles and pedestrian injury severity in motor vehicle crashes. Journal of safety research, 90, 115-127.

VII. APPENDIX

Appendix A

Scatter plots for the developed meta-models

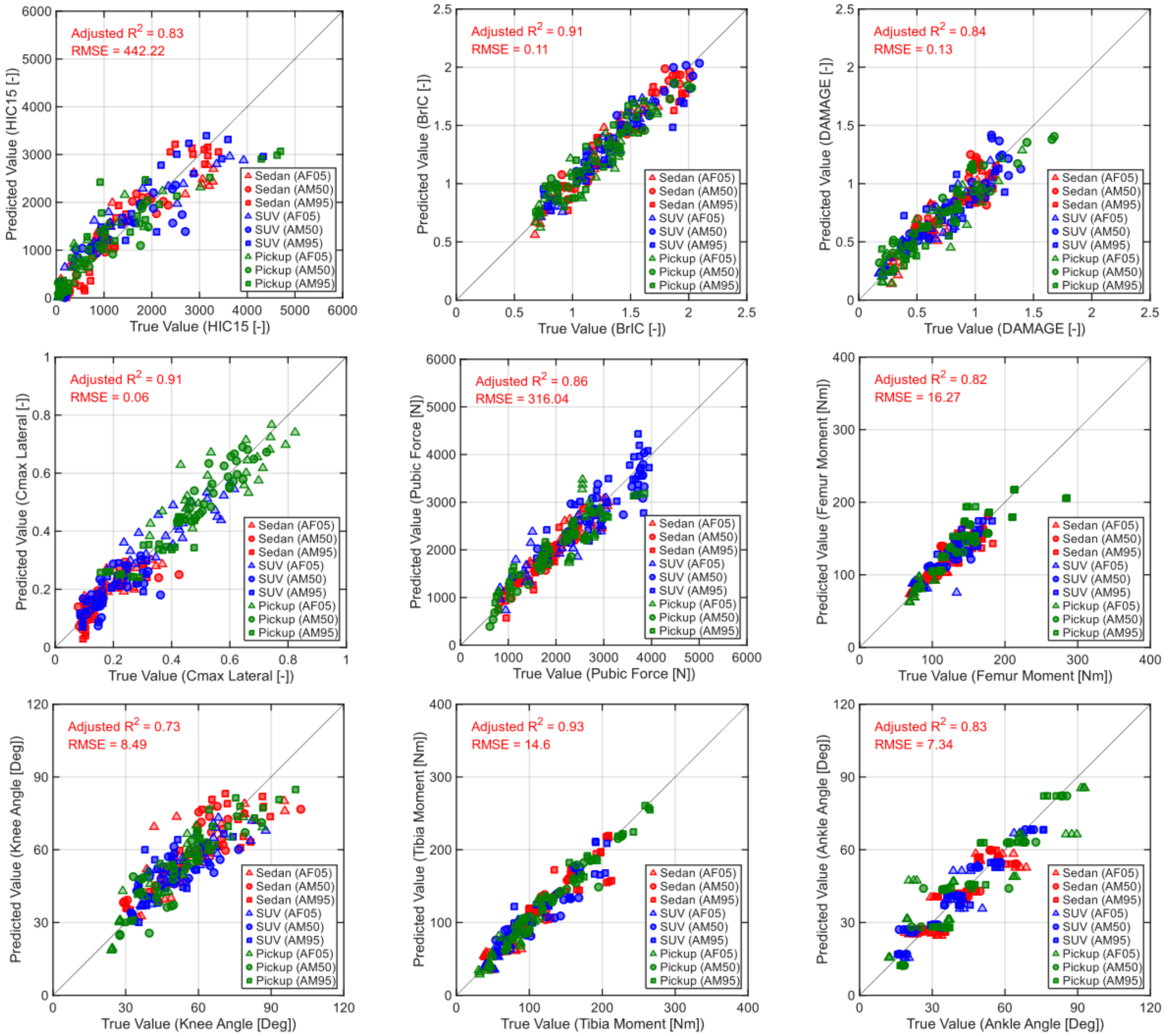

Fig. A1. The predicted performance of the meta-model for nine injury metrics.

Appendix B

Estimated Regression Coefficients

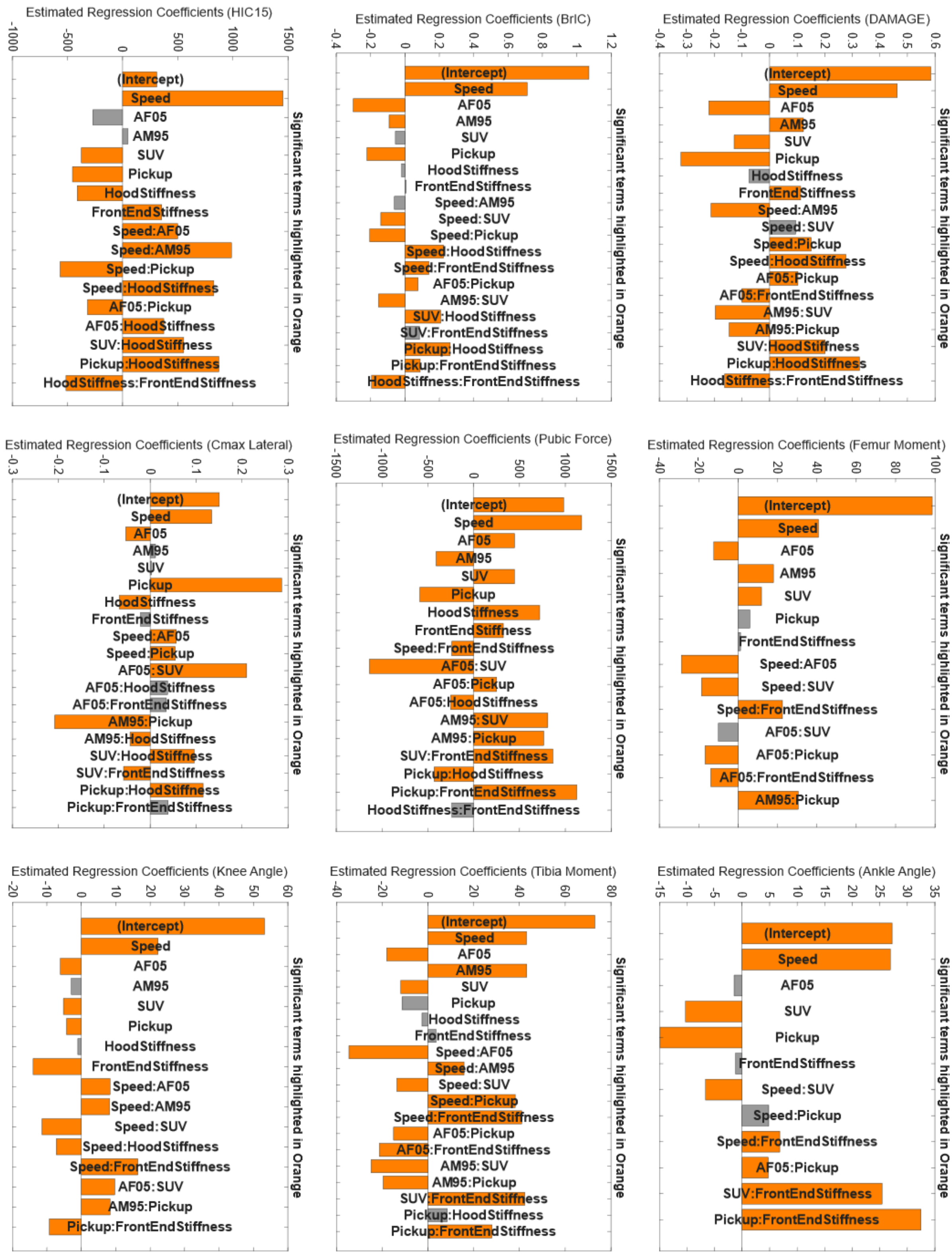

Fig. B1. Estimated regression coefficients for nine meta-models. The symbol ":" denotes a first-order interaction term. Significant terms are highlighted in orange.

Appendix C

Tile Plots

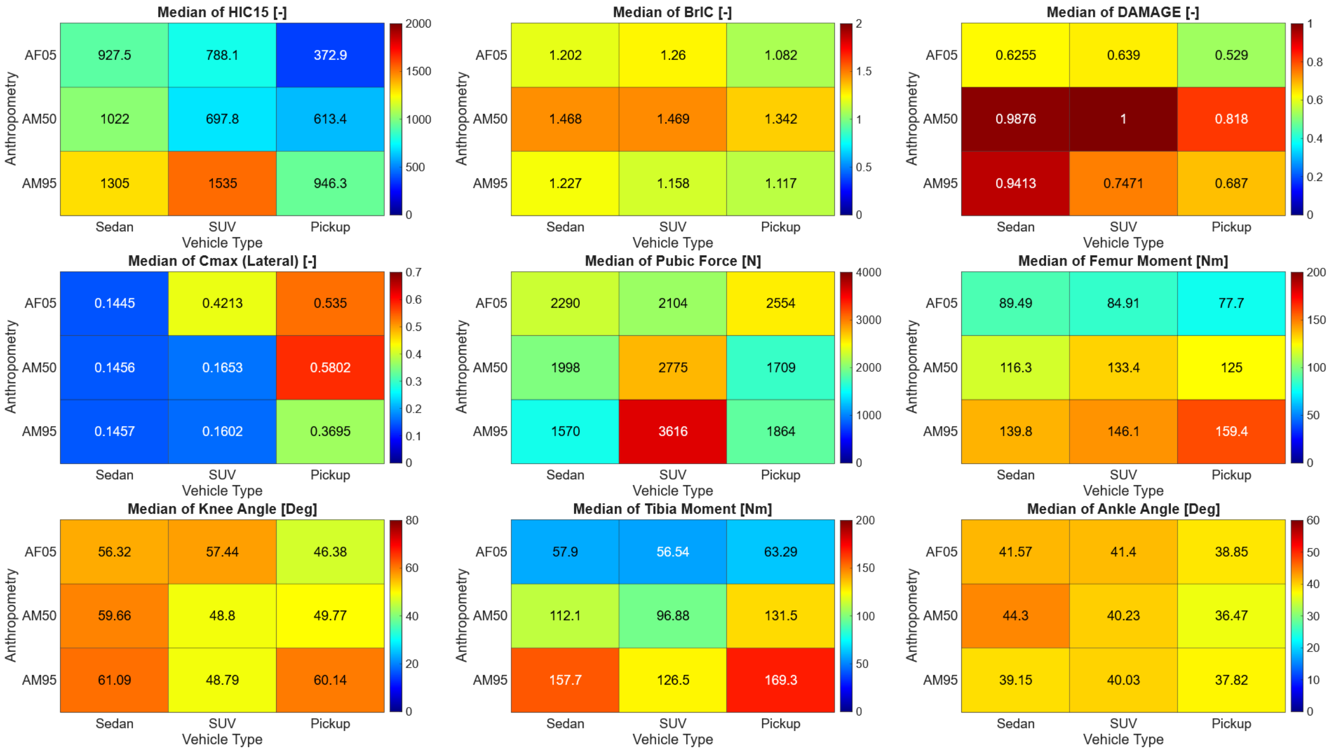

Fig. C1. Median of injury metrics across anthropometry and vehicle type.

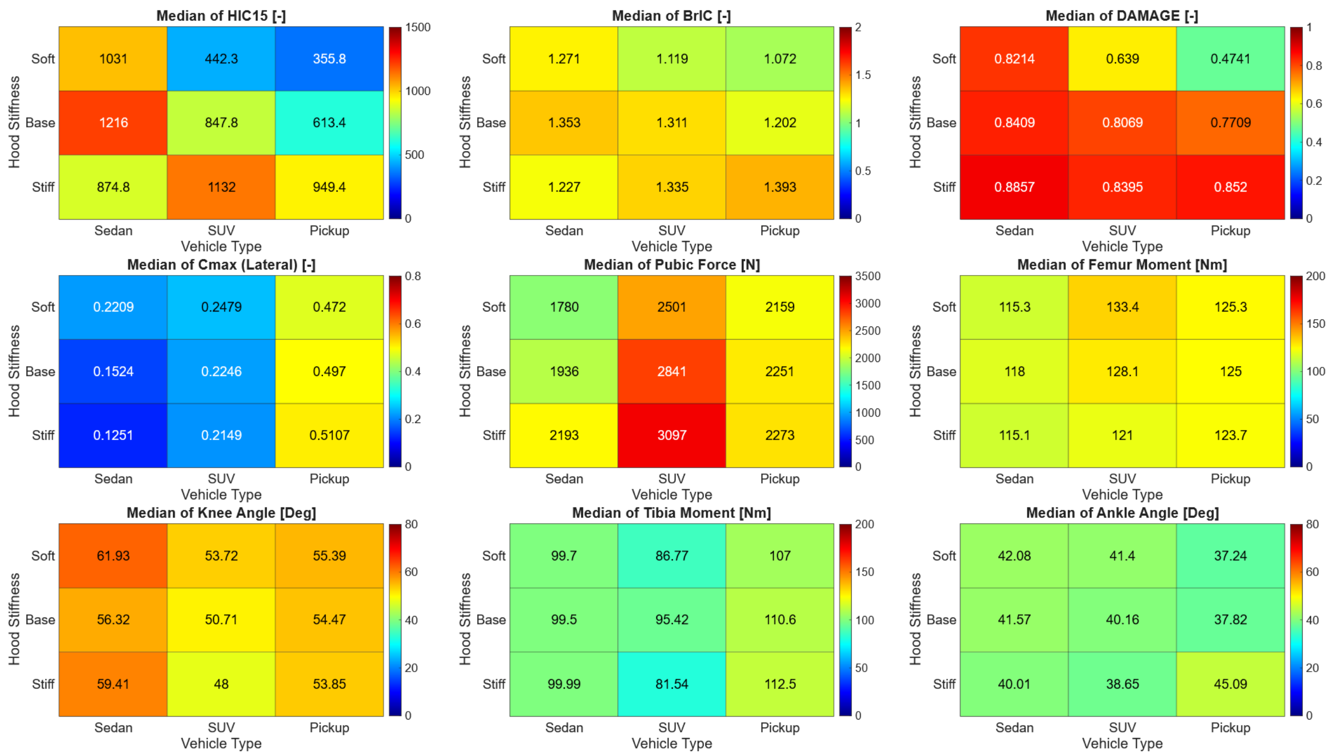

Fig. C2. Median of injury metrics across hood stiffness and vehicle type.

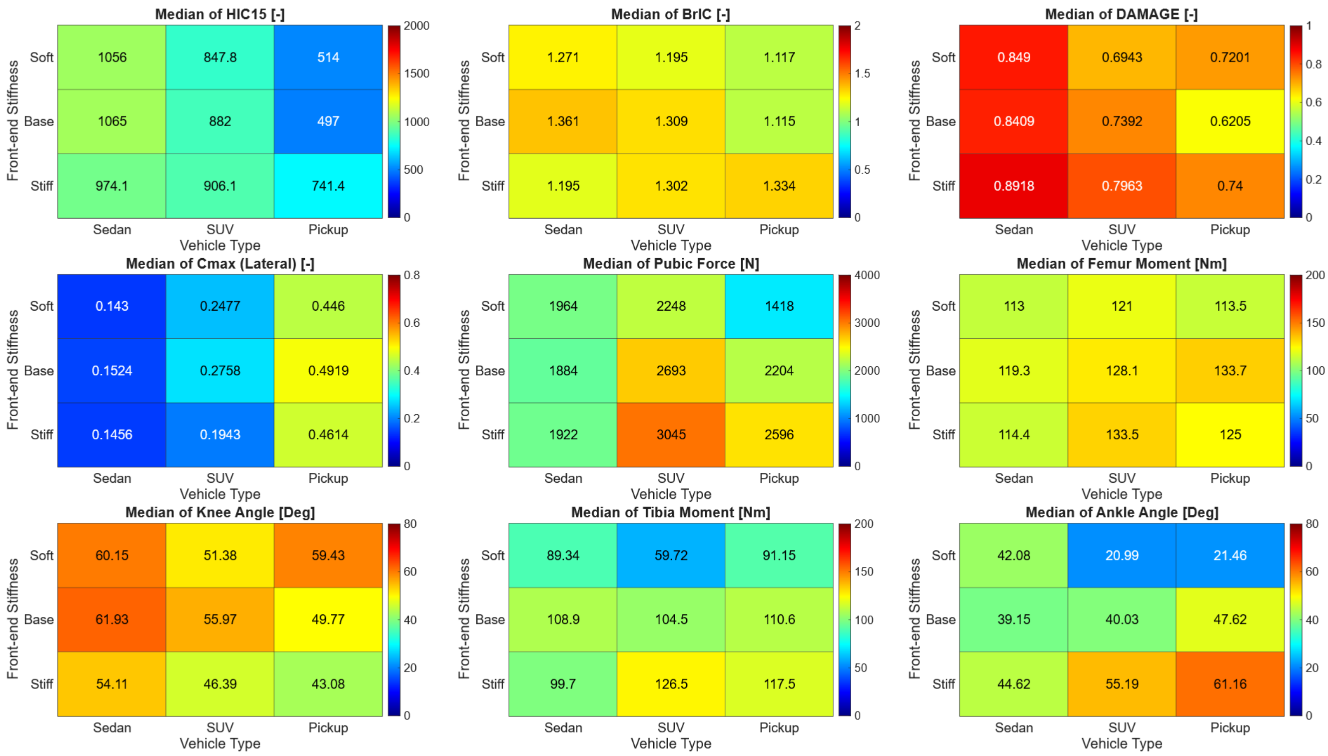

Fig. C3. Median of injury metrics across front-end stiffness and vehicle type.

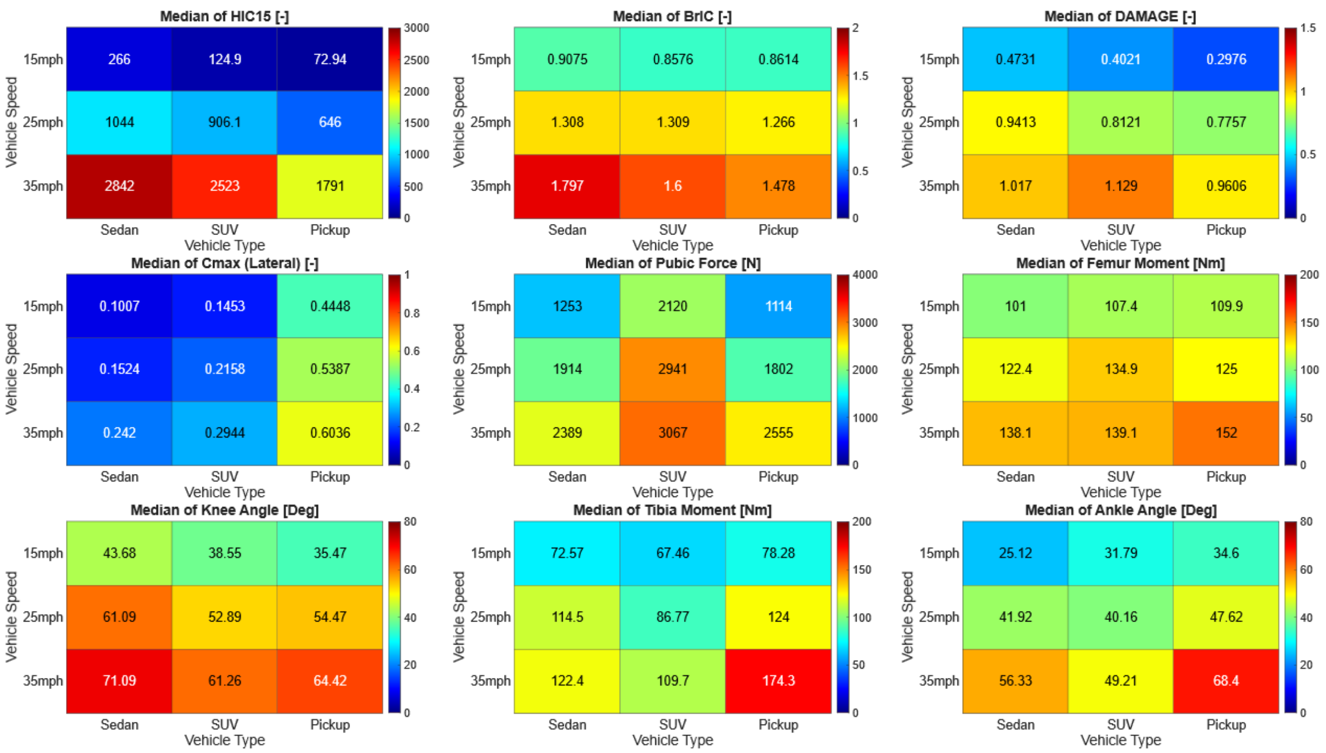

Fig. C4. Median of injury metrics across vehicle speed and vehicle type.

Appendix D

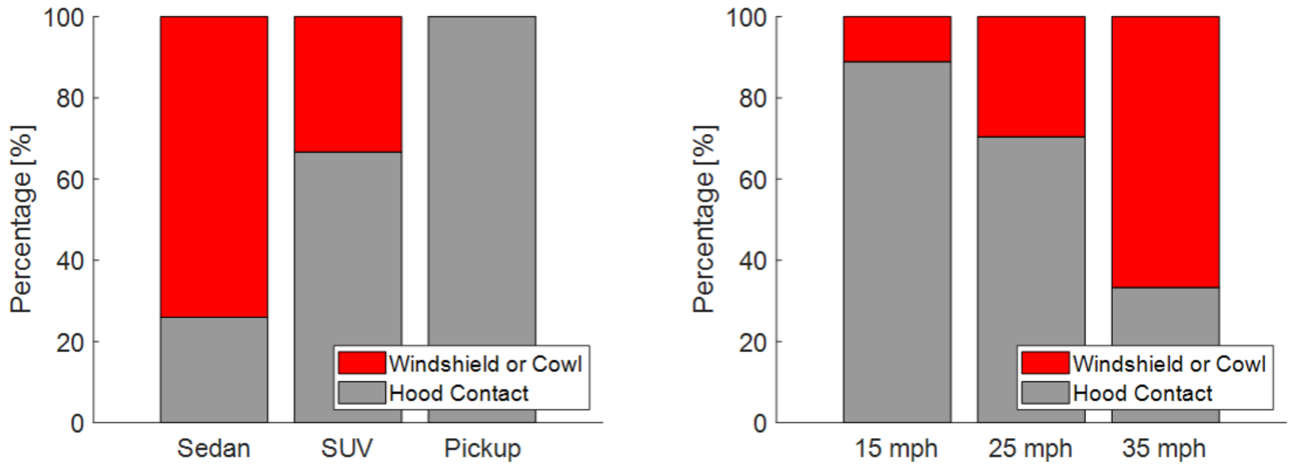

Fig. D1. Head contact distribution for AM50 across vehicle type and vehicle speed.

Appendix E

Vehicle hood and front-end stiffness adjustment.

Silverado – HIC Summary

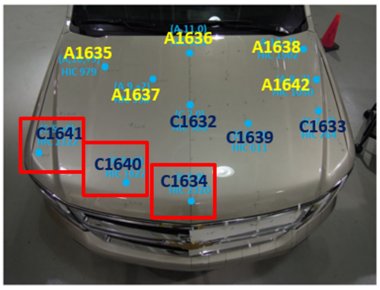

Color	Euro NCAP HIC_{15} range	Euro NCAP Accepted HIC_{15} range
Green	$HIC_{15} < 650$	$HIC_{15} < 722.22$
Yellow	$650 \le HIC_{15} < 1000$	$590.91 \le HIC_{15} < 1111.11$
Orange	$1000 \le HIC_{15} < 1350$	$909.09 \le HIC_{15} < 1500.00$
Brown	$1350 \le HIC_{15} < 1700$	$1227.27 \le HIC_{15} < 1888.89$
Red	$1700 \le HIC_{15}$	$1545.45 \le HIC_{15}$

Test No.	Gird point		HIC Value Soft	Baseline	Stiff
1632	C	7,0	297	696	1747
1633	C	7,-7	493	1072	1704
1634	C	2,0	1375	1689	2662
1635	A	10,5	663	654	1957
1636	A	11,0	486	640	1583
1637	A	9,2	443	452	1117
1638	A	12,-7	606	789	1707
1639	C	6,-3	388	649	1949
1640	C	3,3	1260	1596	2046
1641	C	5,8	1653	1867	2859
1642	A	9,-7	251	1283	2024

High HIC values in the area near the hood edge

Fig. E1. The stiffness adjustment for the Chevrolet Silverado based on HIC15 score result.

Rogue – HIC Summary

Color	Euro NCAP	
	HIC_{15} range	Accepted HIC_{15} range
Green	$HIC_{15} < 650$	$HIC_{15} < 722.22$
Yellow	$650 \leq HIC_{15} < 1000$	$590.91 \leq HIC_{15} < 1111.11$
Orange	$1000 \leq HIC_{15} < 1350$	$909.09 \leq HIC_{15} < 1500.00$
Brown	$1350 \leq HIC_{15} < 1700$	$1227.27 \leq HIC_{15} < 1888.89$
Red	$1700 \leq HIC_{15}$	$1545.45 \leq HIC_{15}$

			HIC Value		
Test No.	Gird point		Soft	Baseline	Stiff
1601	A	7,0	623	623	623
1602	A	7,-7	383	738	1864
1603	A	2,0	402	746	2256
1604	A	10,5	1069	1060	1759
1605	C	11,0	824	1209	2878
1606	C	9,2	1142	1229	2433
1607	C	12,-7	243	1005	2931
1608	C	6,-3	394	747	2084
1609	C	3,3	1212	1598	2210
1610	C	5,8	401	837	1369
1611	C	9,-7	524	1037	2861

High HIC values in the area near the hood edge

Fig. E2. The stiffness adjustment for the Nissan Rogue based on HIC15 score result.

Camry – HIC Summary

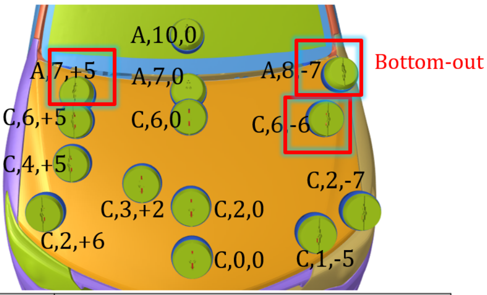

Color	Euro NCAP	
	HIC_{15} range	Accepted HIC_{15} range
Green	$HIC_{15} < 650$	$HIC_{15} < 722.22$
Yellow	$650 \leq HIC_{15} < 1000$	$590.91 \leq HIC_{15} < 1111.11$
Orange	$1000 \leq HIC_{15} < 1350$	$909.09 \leq HIC_{15} < 1500.00$
Brown	$1350 \leq HIC_{15} < 1700$	$1227.27 \leq HIC_{15} < 1888.89$
Red	$1700 \leq HIC_{15}$	$1545.45 \leq HIC_{15}$

		HIC Value		
Grid point		Soft	Baseline	Stiff
A	10,0	393	412	412
A	7,5	1889	425	2250
A	7,0	598	292	2154
A	8,-7	1100	542	1088
C	6,5	250	497	2004
C	6,0	259	647	2223
C	6,-6	807	481	2132
C	4,5	292	489	2244
C	3,2	202	412	1601
C	2,0	201	478	2432
C	2,-7	701	841	2216
C	2,6	568	725	1767
C	0,0	440	798	2076
C	1,-5	710	767	1836

Fig. E3. The stiffness adjustment for the Toyota Camry based on HIC15 score result.

Silverado – Upper Legform

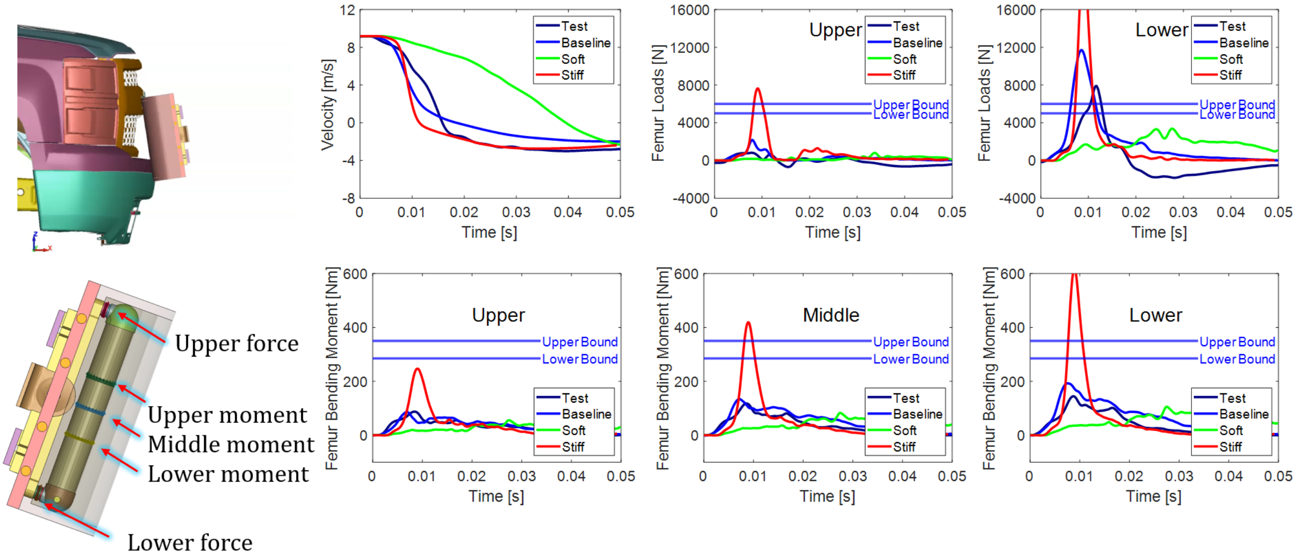

Fig. E4. The stiffness adjustment for the Chevrolet Silverado based on force and moments in Upper legform.

Rogue – Upper legform

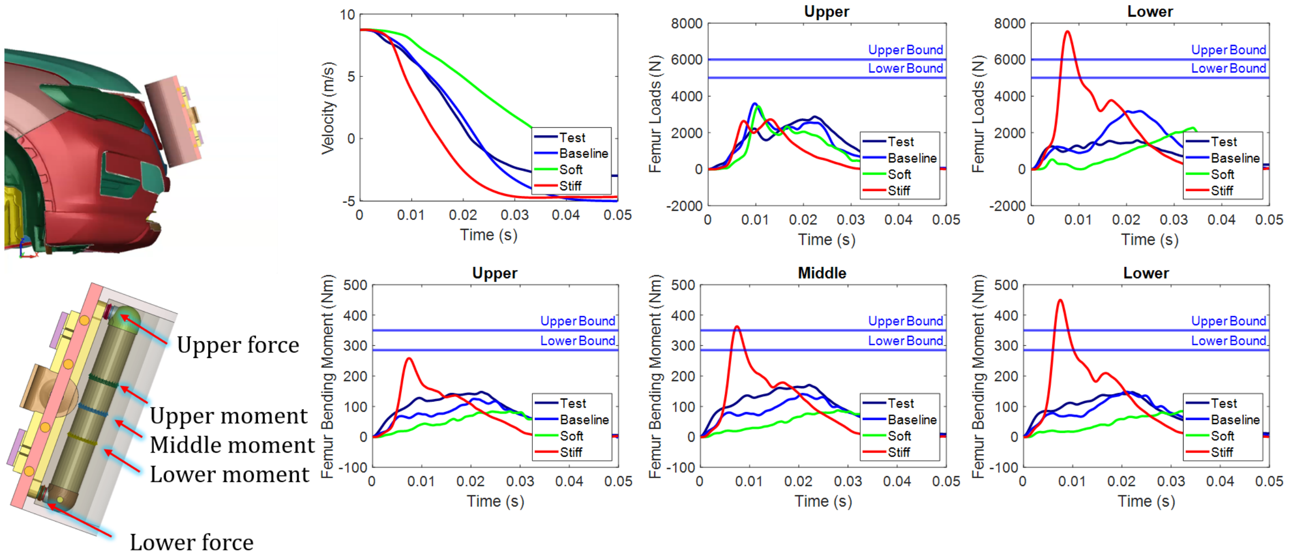

Fig. E5. The stiffness adjustment for the Nissan Rogue based on force and moments in Upper legform.

Camry – Upper legform

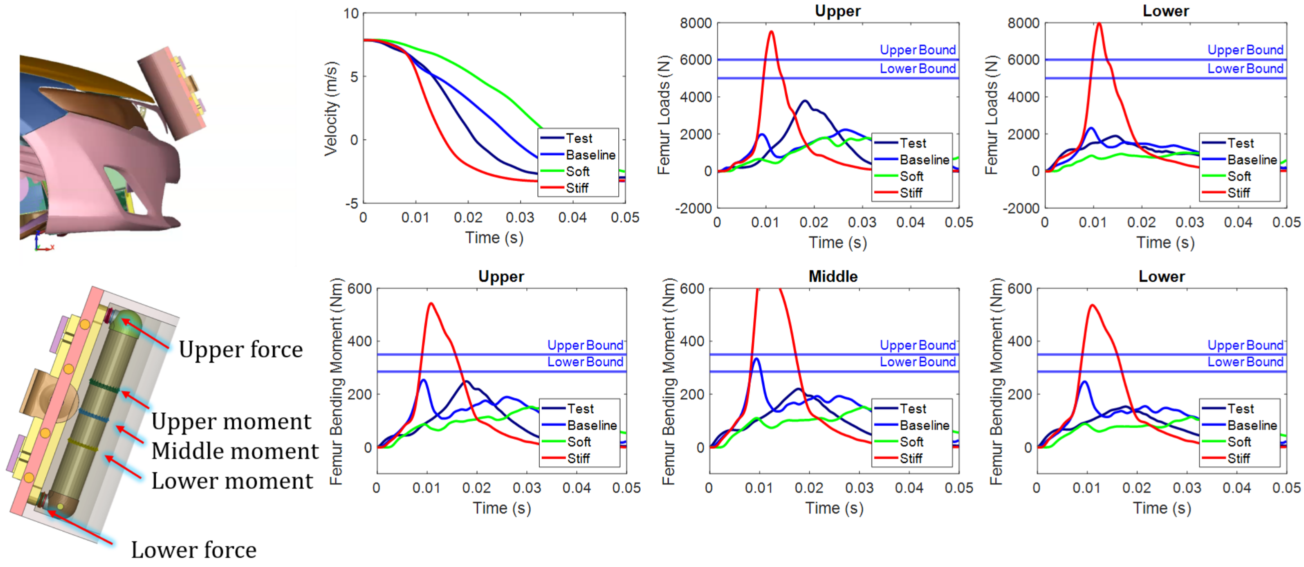

Fig. E6. The stiffness adjustment for the Toyota Camry based on force and moments in Upper legform.

Silverado – Lower Legform

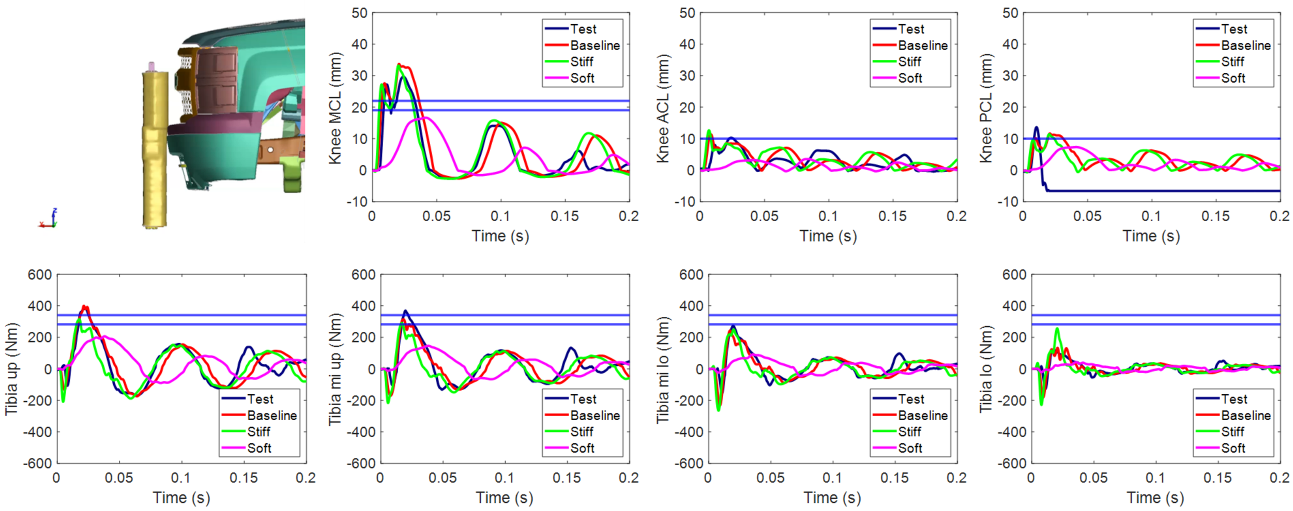

Fig. E7. The stiffness adjustment for the Chevrolet Silverado based on knee displacement and tibia moments.

Rogue – Lower Legform

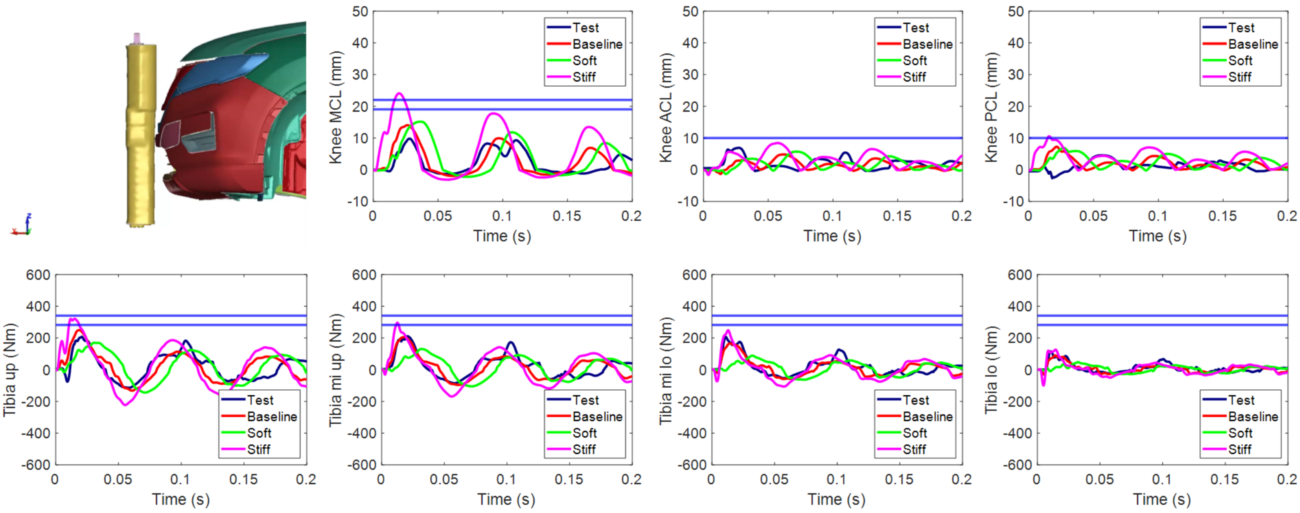

Fig. E8. The stiffness adjustment for the Nissan Rogue based on knee displacement and tibia moments.

Camry – Lower legform

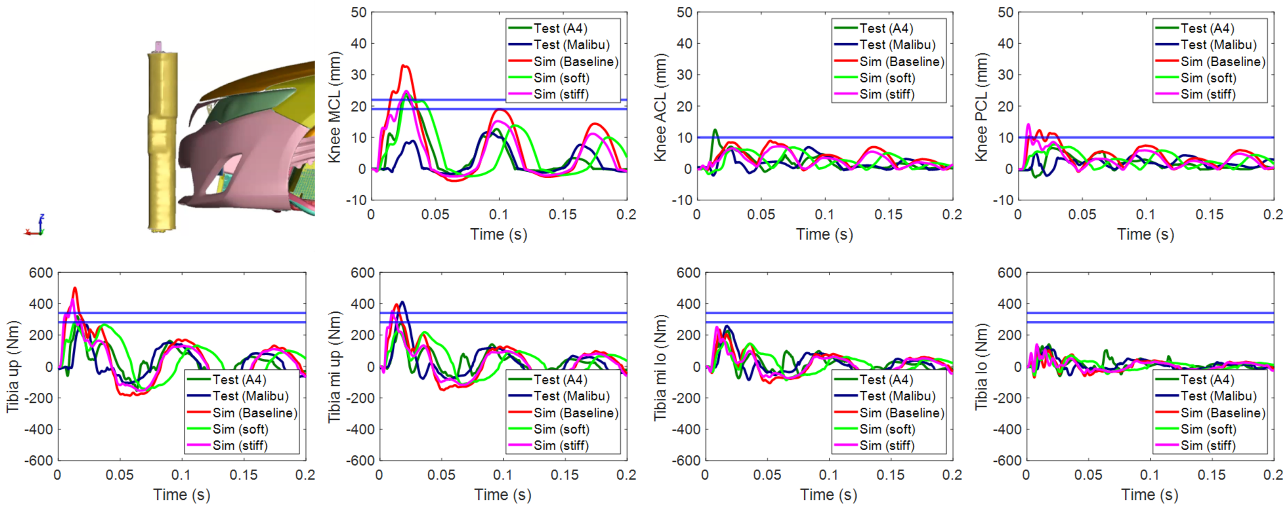

Fig. E9. The stiffness adjustment for the Toyota Camry based on knee displacement and tibia moments.

Appendix F

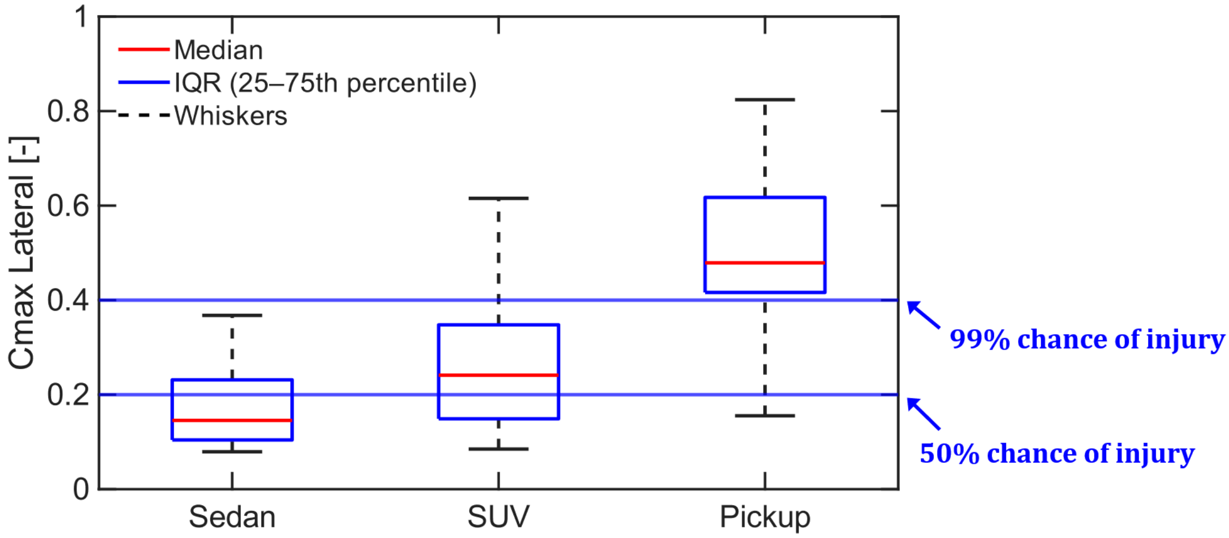

Fig. F1. The distribution of Cmax across all anthropometries for each vehicle type. The 99% and 50% injury probability values were calculated using a published AIS 3+ level injury risk function for 45 year old pedestrian.

Appendix G

To check whether these three vehicles appropriately represent their categories, Principal Component Analysis (PCA) was performed [39]. Nine geometric parameters (Fig. G2) derived from a large dataset [40] were used for this analysis. The PCA function in the statistical toolbox of MATLAB (R2025b, The MathWorks Inc., Natick, MA) was used for this analysis. PCA returns principal components (PCs) which define a new basis that best represents the variability in the dataset, along with corresponding variances that indicate the measure of the importance of each PC. The PCs are ranked in descending order of variance. Therefore, the first PC represents the most important basis.

The PCA results show that the first three PCs account for approximately 75% of the geometric variation (Fig. G1). The physical interpretations of the PCs are as follows:

- PC1 (40%) primarily represents vehicle height. Hood leading edge height, windshield height, and ground clearance are the dominant parameters. Higher PC1 values correspond to vehicles with higher hood leading edge, higher windshield, and higher ground clearance, which are typically observed in large SUVs and pickup trucks.
- PC2 (20%) is associated with front-end shape, particularly the slope of front-end and length of the hood. Bumper leading edge distance, leading edge angle, and hood length are the most influential parameters. Higher PC2 values indicate blunt front-end and longer hood.
- PC3 (15%) is mainly explained by windshield angle, and windshield length. Since this study focuses on front-end geometry, PC3 is considered less relevant for this study.

Based on this interpretation, PC1 and PC2 were selected to visualize the distribution of 4,472 vehicle geometries and three specific vehicles (2015 Toyota Camry, 2020 Nissan Rogue, and 2014 Chevrolet Silverado). Fig. G1 shows the PC1-PC2 space, where seven clusters were identified using k-means clustering, with cluster centroids marked by "X". The 2015 Toyota Camry (red star) is located within the orange cluster, representing vehicles with relatively low hood leading edge heights and moderately sloped front-end. The 2020 Nissan Rogue (blue star) shows higher PC1 values than the Camry, indicating a taller vehicle geometry. The 2014 Chevrolet Silverado (green star) falls within the green cluster, representing high hood leading edge and blunt front-end geometry. Based on this PC1-PC2 space, the Toyota Camry can be classified as a mid-sized sedan, the Nissan Rogue as a small SUV, and the Chevrolet Silverado as a pickup truck with blunt front-end geometry.

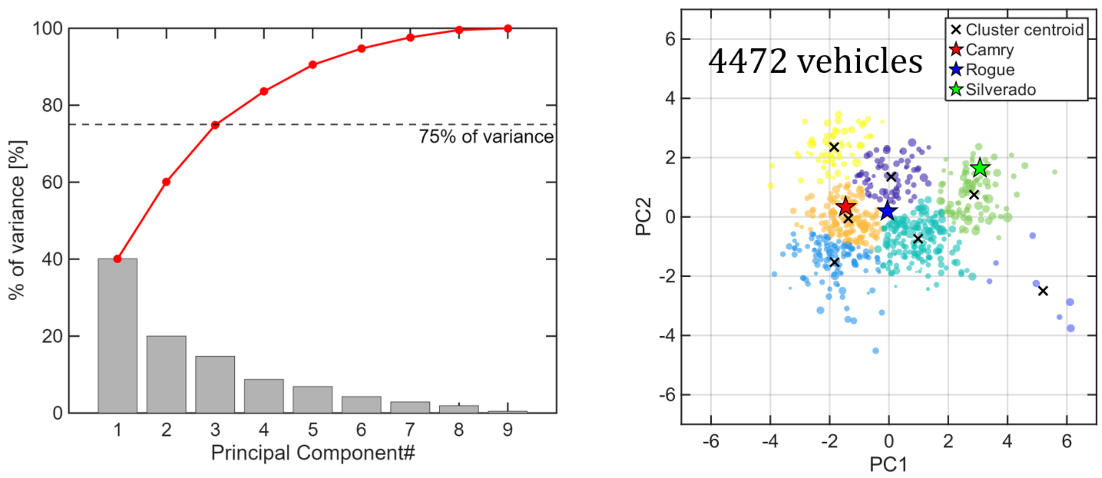

Fig. G1. Percentage of variance explained by principal components (Left): bar graph explains % of the variance, and the red line is cumulative plot of the % of the variance. PC1-PC2 space (right): the distribution of 4,472 vehicle geometries and three specific vehicles.

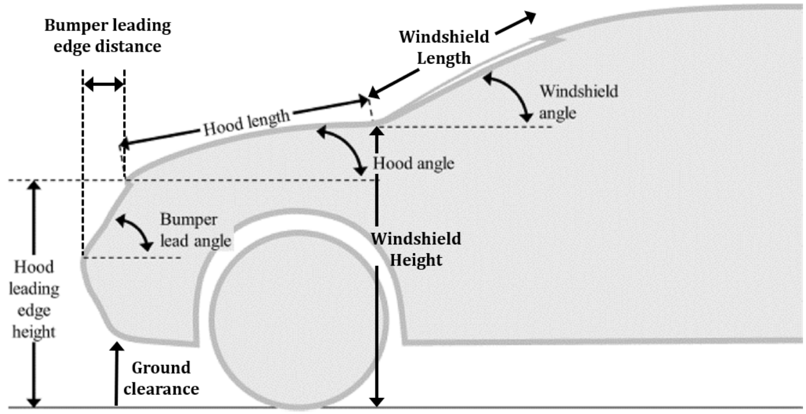

Fig. G2. Vehicle front-end profile parameters adapted from [40]. Nine geometric parameters were used for PCA analysis.